Физико-технический институт им. А. Ф. Иоффе
Российской академии наук

Международная зимняя школа по физике полупроводников

2004

Научная программа и тезисы докладов

С.-Петербург – Зеленогорск
27 февраля – 1 марта 2004 года

Светлой памяти профессора И. П. Ипатовой,
внесшей неоценимый вклад
в организацию и проведение зимних школ ФТИ, посвящается

Организатор

Физико-технический институт им. А. Ф. Иоффе
Российской академии наук

Руководство и организация школы

Р. В. Парфеньев, *директор школы*

А. Г. Забродский, *зам. директора школы,*
председатель оргкомитета

В. И. Перель, *председатель программного комитета*

Е. Л. Ивченко, *программный комитет*

И. П. Ипатова, *программный комитет*

П. С. Копьев, *программный комитет*

О. М. Сресели, *программный комитет*

Р. А. Сурис, *программный комитет*

А. М. Бойко, *сессия молодых ученых*

Л. Ф. Гребеновская, *оргкомитет*

Е. В. Ильина, *оргкомитет*

Т. В. Рогозина, *оргкомитет*

А. Ю. Маслов, *издательская работа*

В. Л. Шубин, *техническое обеспечение*

Т. В. Тиснек, *секретарь оргкомитета*

Спонсоры

Российский фонд фундаментальных исследований
Министерство промышленности, науки и технологий Российской Федерации
Физико-технический институт им. А. Ф. Иоффе
Российской академии наук

Научная программа

Пятница, 27 февраля

Суббота, 28 февраля

Воскресенье, 29 февраля

Понедельник, 1 марта

* Звездочкой отмечены лекции, авторы которых не представили необходимые материалы к оговоренному сроку.

Multiple scattering effects in rough surface scattering

A. A. Maradudin

Department of Physics and Astronomy and Institute for Surface and Interface Science
University of California, Irvine, CA 92697, USA

The first theoretical study of the scattering of light from a randomly rough surface was carried out by Mandel'shtam in 1913, in the context of the scattering of light from the surface of a liquid [1]. These calculations were carried out on the basis of a single-scattering approximation, and for more than 70 years after the work of Mandel'shtam single-scattering approaches continued to underlie theoretical investigations of rough surface scattering. These approaches consisted either of small-amplitude perturbation theory [2], in which the amplitude of the scattered or transmitted field was calculated to first order in the surface profile function — the function that gives the departure of a random surface from a planar surface at each point of the latter — or of the Kirchhoff approximation [3], in which the light is assumed to be scattered from and transmitted through the plane tangent to each point of the random surface.

In 1985, however, it was predicted theoretically on the basis of a multiple-scattering calculation of the scattering of p-polarized (transverse magnetic) light from a one-dimensional weakly rough random metal surface that the angular dependence of the intensity of the light scattered incoherently (diffusely) displays a well-defined peak in the retroreflection direction [4]. This is a weak localization effect that is caused by the coherent interaction of the multiply-scattered, p-polarized, surface electromagnetic waves — surface plasmon polaritons — supported by the vacuum metal interface with their reciprocal partners. This effect was observed experimentally two years later [5], in experiments in which, however, metal surfaces considerably rougher than those for which the theory or Ref. [4] is valid were used. These results stimulated the development of computational approaches for calculating the scattering of light from large-amplitude, large slope, random surfaces, and searches for additional phenomena that reveal themselves only when multiple scattering is taken into account in these approaches, activities that continue to this day.

In this lecture some of the techniques that have been used to investigate multiple-scattering phenomena in rough surface scattering are outlined, and ef-

fects obtained by their use are described. Where experimental confirmations of the latter exist, they, too, are presented.

The most widely studied weak localization effect in rough surface scattering studied both theoretically and experimentally is the enhanced backscattering effect described above. In the earliest theoretical investigation of it [4] for the scattering of p-polarized light from weakly rough one-dimensional randomly rough metal surfaces, an infinite-order perturbation theory (the solution of a Bethe–Salpeter equation for a two-particle Green's function) that exploited the existence of surface plasmon polaritons at the vacuum-metal interface, was used to calculate the mean differential reflection coefficient. Subsequently, it was shown [6] that if small-amplitude perturbation theory is used for this purpose, it is necessary to work to fourth order in the surface profile function in calculating the mean differential reflection coefficient in order for this effect to reveal itself. Recent perturbative calculations of this effect have included terms of sixth order in the surface profile function [7], and even terms of eighth order [8]. Enhanced backscattering due to the coherent interference of multiply-scattered surface plasmon polaritons with their reciprocal partners in which the surface plasmons scatter from the same points on the surface but in the reverse order, was observed in a clever experiment by West and O'Donnell in 1995 [9] that was analyzed theoretically by Maradudin *et al.* [10].

To deal with scattering from large-amplitude, large-slope one-dimensional randomly rough surfaces, computer simulation approaches were developed [11, 12, 13]. Among other results these methods showed that enhanced backscattering can be observed in the scattering of s-polarized (transverse electric) light from a sufficiently rough metal surface [13]. This is not the case in the scattering of s-polarized light from a weakly rough metal surface, because the latter does not support s-polarized surface plasmon polaritons.

Computer simulation calculations of the scattering of scalar plane waves from two-dimensional randomly rough Dirichlet [14, 15] and Neumann [16] surfaces were carried out, as well as such calculations of the scattering of electromagnetic (vector) waves from two-dimensional perfectly conducting [17] and metallic [18] surfaces.

If one compares the successive terms in the expansion in powers of the surface profile function of the amplitude for the transmission of p-polarized light through a thin, free-standing metal film, whose illuminated surface is a weakly rough one-dimensional random surface, with the corresponding expansion for the scattering amplitude, one finds that the denominators, and hence the poles, in both expansions are the same. These poles give the dispersion relation for the two surface electromagnetic waves supported by the film that are responsible for enhanced

backscattering from the film. Consequently, one might expect that an analogous effect should occur in transmission. This expectation was confirmed theoretically in [19], where it was shown that the angular dependence of the intensity of the light transmitted incoherently displays a well-defined peak in the antispecular direction. This peak was subsequently observed experimentally [20].

When the scattering structure with a randomly rough surface supports two or more surface or guided waves, as does the free-standing metal film mentioned in the preceding paragraph, or a dielectric film deposited on a metal substrate, additional features can arise in the angular dependence of the intensity of the light scattered from it or transmitted through it, namely satellite peaks [21]. These are also multiple-scattering effects that arise due to the fact that the scattering structure supports two or more modes, with different wave numbers, at the frequency ω of the incident light. Thus, if the wavenumbers of the $N(\geq 2)$ modes supported by the structure are $k_1(\omega), k_2(\omega), \ldots, k_N(\omega)$, peaks will occur at scattering angles θ_s measured clockwise from the normal to the mean surface, given by $\sin\theta_s = -\sin\theta_0 \pm(\omega/c)[k_m(\omega) - k_n(\omega)]$, where θ_0 is the angle of incidence, measured counterclockwise from the normal to the mean surface. When $m = n$ the peak is the enhanced backscattering peak, when $m \neq n$, the peaks are satellite peaks. These satellite peaks have now been observed experimentally [22]. The satellite peaks that can arise in transmission have yet to be observed.

In a series of papers published in 1987 [23] E. Wolf considered radiation from a three-dimensional quasihomogeneous source and showed that if the spectral coherence of the source i.e. the correlation in the fluctuations of the source, is appropriately chosen, the spectrum of the emitted radiation can be redshifted or blueshifted with respect to that of the source, even when the source is at rest with respect to the observer, and the radiation propagates in free space. There is an analogy between scattering and radiation that has its origin in the following circumstances. In the scattering of polychromatic light from a static random medium the different frequency components of the incident light, which are scattered in any particular direction, will be scattered with different strengths. Consequently, the spectrum of the scattered light will differ from that of the incident light, even though the different frequency components are uncorrelated. The possibility of generating a spectral redistribution by scattering is analogous to the possibility of generating a spectral redistribution in light emitted from a source caused by correlations in the fluctuations of the source. The only difference is that in scattering one is dealing with secondary sources, namely with the polarization induced in the scattering medium by the incident field. The induced polarization, in general, is correlated over finite distances of the scattering medium, and thus imitates correlations in primary sources. This analogy between scattering and radiation

prompted theoretical [24, 25] and experimental [25, 26] investigations of spectral redistributions of light scattered from randomly rough surfaces that showed that the spectrum of the scattered light indeed differs from that of the incident light.

Up to now I have considered only the intensity of the light scattered from, or transmitted through, a randomly rough surface, namely a second moment of the scattered field. Recently, angular intensity correlation functions of light scattered from randomly rough surfaces have begun to be studied both theoretically and experimentally. These are correlation functions of the type $\langle \delta I(q|k) \delta I(q'|k') \rangle$, where $\delta I(q|k) = I(q|k) - \langle I(q|k) \rangle$, and the angle brackets denote an average over the ensemble of realizations of the surface profile. They represent a fourth moment of the scattered field. $I(q|k)$ is the intensity with which an incident plane wave whose wave vector has a component k parallel to the mean scattering surface is scattered into a plane wave whose wave vector has a component q parallel to the mean scattering surface. These wavenumbers are related to angles of incident θ_0 and scattering θ_s by $k = (\omega/c) \sin\theta_0$, $q = (\omega/c) \sin\theta_s$, $k' = (\omega/c) \sin\theta_0'$, $q' = (\omega/c) \sin\theta_s'$. The theoretical calculations, which take multiple-scattering processes into account, have predicted a memory effect and a reciprocal memory effect, as well as a new correlation function that exists when the scattered field obeys complex Gaussian statistics and vanishes when it obeys circular complex Gaussian statistics [27, 28]. These angular intensity correlation functions have been observed in recent experiments [29].

When highly intense light is incident on a metal surface second harmonic light is generated in reflection. When the metal surface is randomly rough, weak localization effects are present in the angular dependence of the intensity of the second harmonic light. When the surface is weakly rough and is characterized by a power spectrum that enhances the excitation of surface plasmon polaritons of frequency 2ω, by incident light of frequency ω, computer simulation and small-amplitude perturbation theory calculations of the second harmonic intensity predict a dip in the retroreflection direction for all angles of incidence [30, 31]. This prediction is in agreement with experimental results presented in [32]. When the surface roughness is characterized by a power spectrum that enhances the excitation of surface plasmon polaritons of frequency ω by incident light of frequency ω, peaks are predicted at scattering angles defined by $q = k \pm k_{sp}(\omega)$ [31], where $k = (\omega/c) \sin\theta_0$, $q = (w/c) \sin\theta_s$, and $k_{sp}(\omega)$ is the wavenumber of surface plasmon polaritons of frequency ω. They are associated with the resonant nonlinear interaction of the excited surface plasmon polariton with the incident light. These peaks are observed in the experimental results of [33]. In the case of second harmonic generation from strongly rough metal surfaces, computer simulation calculations[34] show dips in the retroreflection direction in the angular dependence of the scattered light at the

harmonic frequency, in agreement with the experimental results presented in [35].

The preceding discussion does not cover all the weak localization effects predicted theoretically and observed experimentally when multiple-scattering effects are taken into account in studies of rough surface scattering. Yet they illustrate the richness of the phenomena multiple scattering produces, and raise the expectation that there are still more to be discovered.

Bibliography

[1] L. I. Mandel'shtam, Ann. Physik **41**, 609 (1913).
[2] S. O. Rice, Commun. Pure Appl. Math. **4**, 351 (1951).
[3] P. Beckmann and A. Spizzichino, *The Scattering of Electromagnetic Waves from Rough Surfaces* (Pergamon, Oxford, 1963).
[4] A. R. McGurn, A. A. Maradudin, and V. Celli, Phys. Rev. B**31**, 4866 (1985).
[5] E. R. Méndez and K. A. O'Donnell, Opt. Commun. **61**, 95 (1987); K. A. O'Donnell and E. R. Méndez, J. Opt. Soc. Am. A**4**, 1194 (1987).
[6] A. A. Maradudin and E. R. Méndez, Appl. Opt. **32**, 3335 (1993).
[7] K. A. O'Donnell, C. S. West, and E. R. Méndez, Phys. Rev. B**57**, 13209 (1998).
[8] K. A. O'Donnell, J. Opt. Soc. Am. A**18**, 1507 (2001).
[9] C. S. West and K. A.O'Donnell, J. Opt. Soc. Am. A**12**, 390 (1995).
[10] A. A. Maradudin, A. R. McGurn, and E. R. Méndez, J. Opt. Soc. Am. A**12**, 2500 (1995).
[11] M. Nieto-Vesperinas and J. M. Soto-Crespo, Opt. Lett. **12**, 979 (1987).
[12] A. A. Maradudin, E. R. Méndez, and T. Michel, Opt. Lett. **14**, 151 (1989).
[13] A. A. Maradudin, T. Michel, A. R. McGurn, and E. R. Méndez, Ann. Phys. (N.Y.) **203**, 255 (1990).
[14] P. Tran and A. A. Maradudin, Phys. Rev. B**45**, 3936 (1992).
[15] C. Macaskill and B. J. Kachoyan, Appl. Opt. **32**, 2839 (1993).
[16] P. Tran and A. A. Maradudin, Appl. Opt. **32**, 2848 (1993).
[17] P. Tran, V. Celli, and A. A. Maradudin, J. Opt. Soc. Am. A**11**, 1686 (1994).
[18] P. Tran and A. A. Maradudin, J. Opt. Commun. **110**, 269 (1994).
[19] A. R. McGurn and A. A. Maradudin, Opt. Commun. **72**, 279 (1989).
[20] V. Celli, P. Tran, A. A. Maradudin, Jun Lu, T. Michel, and Zu-Han Gu, in *Laser Optics of Condesned Matter*, Vol. 2, eds. E. Garmire, A. A. Maradudin, and K. K. Rebane (Plenum, New York, 1991), p. 315.
[21] V. Freilikher, M. Pustilnik, I. Yurkevich, and A. A. Maradudin, Opt. Commun. **110**, 263 (1994).
[22] E. R. Méndez, E. I. Chaikina, and H. M. Escamilla, Opt. Lett. **24**, 705 (1999); H. M. Escamilla, E. R. Méndez, and E. I. Chaikina, J. Opt. Soc. Am. A**18**, 1122 (2001).
[23] E. Wolf, Nature **326**, 363 (1987); Phys. Rev. Lett. **58**, 2646 (1987); Opt. Commun. **62**, 12 (1987).
[24] T. A. Leskova, A. A. Maradudin, A. V. Shchegrov, and E. R. Méndez, Phys. Rev. Lett. **79**, 1010 (1997).

[25] E. I. Chaikina, H. M. Escamilla, and E. R. Méndez, submitted to Opt. Commun.
[26] Zu-Han Gu, SPIE **4447**, 109 (2001).
[27] V. Malyshkin, A. R. McGurn, T. A. Leskova, A. A. Maradudin, and M. Nieto-Vesperinas, Opt. Lett. **22**, 946 (1997); Waves in Random Media **7**, 479 (1997).
[28] T. A. Leskova, I. Simonsen, and A. A. Maradudin, Waves in Random Media **12**, 307 (2002).
[29] C. S. West and K. A. O'Donnell, Phys. Rev. B**59**, 2393 (1999).
[30] M. Leyva-Lucero, E. R. Méndez, T. A. Leskova, A. A. Maradudin, and Jun Q. Lu, Opt. Lett. **21**, 1809 (1996).
[31] T. A. Leskova, A. A. Maradudin, and E. R. Méndez, in *Optical Properties of Nanostructured Random Media*, ed. V. M. Shalaev (Springer-Verlag, NY, 2002), p. 359.
[32] K. A. O'Donnell, R. Torre, and C. S. West, Opt. Lett. **21**, 1738 (1996).
[33] K. A. O'Donnell, R. Torre, and C. S. West, Phys. Rev. B**55**, 7985 (1997).
[34] M. Leyva-Lucero, E. R. Méndez, T. A. Leskova, and A. A. Maradudin, Opt. Commun. **161**, 79 (1999).
[35] K. A. O'Donnell and R. Torre, Opt. Commun. **138**, 341 (1997).

Designer surfaces

A. A. Maradudin
Department of Physics and Astronomy and Institute for Surface and Interface Science
University of California, Irvine, CA 92697, USA

In many practical situations it is desirable to have optical diffusers with specific light scattering properties. For example, a nonabsorbing diffuser that scatters light uniformly within a specified range of scattering angles, and produces no scattering outside this range, could have applications in projection systems where one wishes to illuminate a screen with uniform intensity but not to waste light by illuminating outside the boundaries of the screen. We will call such an optical element a *band-limited uniform diffuser*. Band-limited uniform diffusers can also be useful in microscope illumination systems, in the fabrication of displays and projection screens, and in Fourier transform holography. A random surface that acts as a band-limited uniform diffuser would consequently be a useful optical element. Lambertian diffusers, which produce a scattered intensity that is proportional to the cosine of the polar scattering angle, are frequently used in the optical industry, e.g. for calibrating scatterometers [1]. Such diffusers have the property that their radiance or luminance is the same in *all* scattering directions. In the visible region of the optical spectrum volume disordered media, e.g. compacted powdered barium sulfate, and freshly smoked magnesium oxide are used as Lambertian diffusers [2]. However, this type of diffuser is inapplicable in the infrared

region due to its strong absorption and the presence of a specular component in the scattered light, in this frequency range. The design of a random surface that acts as a Lambertian diffuser, especially in the infrared region of the optical spectrum is therefore a desirable goal, and one that has been regarded as difficult to achieve [3]. Yet another example is provided by the fact that in the scattering of light from a random surface the multiple-scattering processes that give rise to such interesting weak localization effects as enhanced backscattering, enhanced transmission, satellite peaks, and new angular intensity correlation functions, are accompanied by single-scattering processes on which these, often subtle, effects are superimposed. The design of random surfaces that suppress single-scattering in a suitable range of scattering angles could be useful in increasing the visibility of these effects.

The design of band-limited uniform diffusers, some of which employ one- or two-dimensional random surfaces, has been considered by several authors [4–7]. Diffractive optical elements that scatter light uniformly over specified angular regions have become commercially available [8]. These elements, however, are not random and possess the desired characteristics over only a relatively narrow range of wavelengths. Thus, they are not achromatic. Another kind of diffuser, whose design is based on a randomized microlenslet concept, is also available commercially [9]. Although these holographic light shaping diffusers are achromatic, and possess characteristics that approximate the desired ones, the scattering distribution they produce is not uniform, and they do not have a well-defined maximum angle of scattering.

Despite the interest in this subject, until recently there were no clear procedures reported in the literature for designing and fabricating randomly rough surfaces that behave as band-limited uniform diffusers, or scatter light in other specified ways, and it was unclear what kind of surface statistics were required for the production of such optical elements. In this lecture I will present approaches due to my colleagues and myself to the design and fabrication of one- and two-dimensional randomly rough surfaces that possess the scattering properties described above [10–21] These methods are based on the geometrical optics limit of the Kirchhoff approximation, a single-scattering approximation, for the scattering of scalar plane waves from impenetrable surfaces. However, as we will see, the results obtained by these methods have a significantly wider range of applicability. We have chosen to work with random surfaces in designing optical diffusers that scatter light in a prescribed fashion because, as will be shown, the use of such surfaces leads to a precise algorithm for designing them, something that we have been unable to find in dealing with deterministic surfaces.

I begin by considering one-dimensional random surfaces. The physical system

that is assumed initially consists of vacuum in the region $x_3 > \zeta(x_1)$ and a perfect conductor in the region $x_3 < \zeta(x_1)$. The surface profile function $\zeta(x_1)$ is assumed to be a single-valued function of x_1 that is differentiable and constitutes a random process, but not necessarily a stationary one. The surface $x_3 = \zeta(x_1)$ is illuminated from the vacuum region by an s-polarized plane wave of frequency ω, whose plane of incidence is the x_1x_3-plane. The single nonzero component of the electric field $E_2^>(x_1, x_3; t) = E_2^>(x_1, x_3|\omega)\exp(-i\omega t)$ in the region $x_3 > \zeta(x_1)_{\max}$ is the sum of an incident plane wave and a superposition of outgoing scattered plane waves,

$$E_2^>(x_1, x_3|\omega) = \exp[ikx_1 - i\alpha_0(k)x_3] + \int_{-\infty}^{\infty} \frac{dq}{2\pi} R(q|k)\exp[iqx_1 + i\alpha_0(q)x_3], \quad (1)$$

where $\alpha_0(q) = [(\omega/c)^2 - q^2]^{\frac{1}{2}}$, with $\mathrm{Re}\alpha_0(q) > 0, \mathrm{Im}\alpha_0(q) > 0$.

The differential reflection coefficient, $\partial R/\partial\theta_s$, which is defined in such a way that $(\partial R/\partial\theta_s)d\theta_s$ is the fraction of the total time-averaged incident flux that is scattered into the angular interval $(\theta_s, \theta_s + d\theta_s)$, is given in terms of the scattering amplitude $R(q|k)$ by

$$\frac{\partial R}{\partial\theta_s} = \frac{1}{L_1}\frac{\omega}{2\pi c}\frac{\cos^2\theta_s}{\cos\theta_0}|R(q|k)|^2, \quad (2)$$

where L_1 is the length of the x_1-axis covered by the random surface, while θ_0 and θ_s are the angles of incidence and scattering measured counterclockwise and clockwise from the $+x_3$-axis, respectively, and are related to the wavenumbers k and q by $k = (\omega/c)\sin\theta_0$, $q = (\omega/c)\sin\theta_s$. As we are concerned with the scattering of light from a randomly rough surface, it is the mean differential reflection that we need to calculate. It is defined by

$$\left\langle \frac{\partial R}{\partial\theta_s} \right\rangle = \frac{1}{L_1}\frac{\omega}{2\pi c}\frac{\cos^2\theta_s}{\cos\theta_0}\langle|R(q|k)|^2\rangle, \quad (3)$$

where the angle brackets here and in all that follows denote an average over the ensemble of realizations of the surface profile function.

In the Kirchhoff approximation, which we adopt here for simplicity, the scattering amplitude $R(q|k)$ is given by[11]

$$R(q|k) = -\frac{(\omega/c)^2 + \alpha_0(q)\alpha_0(k) - qk}{\alpha_0(q)[\alpha_0(q) + \alpha_0(k)]} \times \int_{-\infty}^{\infty} dx_1 \exp[-i(q-k)x_1]\exp\{-i[\alpha_0(q) + \alpha_0(k)]\zeta(x_1)\}. \quad (4)$$

The mean differential reflection coefficient in this approximation thus takes the form

$$\left\langle \frac{\partial R}{\partial \theta_s} \right\rangle = \frac{1}{L_1} \frac{\omega}{2\pi c} \frac{1}{\cos\theta_0} \left[\frac{1+\cos(\theta_s+\theta_0)}{\cos\theta_s+\cos\theta_0} \right]^2 \times \int_{-\infty}^{\infty} dx_1 \int_{-\infty}^{\infty} dx_1' \exp[-i(q-k)(x_1-x_1')] \langle \exp\{-ia[\zeta(x_1)-\zeta(x_1')]\} \rangle \quad (5)$$

where, to simplify the notation, we have defined $a = \alpha_0(q) + \alpha_0(k) = (\omega/c)(\cos\theta_s + \cos\theta_0)$.

Our goal is to determine the surface profile function $\zeta(x_1)$ that produces a specified form for $\langle \partial R/\partial\theta_s \rangle$ as a function of θ_s and θ_0. As it stands, the expression given by Eq. (5) is too difficult to invert to obtain $\zeta(x_1)$ in terms of $\langle \partial R/\partial\theta_s \rangle$. To simplify it we pass to the geometrical optics limit of the Kirchhoff approximation by making the change of variable $x_1' = x_1 + u$ in Eq. (5), expanding the difference $\zeta(x_1) - \zeta(x_1+u)$ in powers of u, and retaining only the leading nonzero term:

$$\left\langle \frac{\partial R}{\partial \theta_s} \right\rangle = \frac{1}{L_1} \frac{\omega}{2\pi c} \frac{1}{\cos\theta_0} \left[\frac{1+\cos(\theta_s+\theta_0)}{\cos\theta_s+\cos\theta_0} \right]^2 \int_{-\infty}^{\infty} dx_1 \int_{-\infty}^{\infty} du \exp[i(q-k)u] \times \langle \exp[iau\zeta'(x_1)] \rangle. \quad (6)$$

To proceed, we represent the surface profile function $\zeta(x_1)$ in the form

$$\zeta(x_1) = a_n x_1 + b_n, \quad nb \le x_1 \le (n+1)b, \quad n = 0, \pm 1, \pm 2, \ldots, \quad (7)$$

where b is a characteristic length, and the $\{a_n\}$ are independent, identically distributed random deviates. Therefore, the probability density function (pdf) of a_n, $f(\gamma) = \langle \delta(\gamma - a_n) \rangle$, is independent of n. In order that the surface be continuous at $x_1 = (n+1)b$, the relation

$$b_{n+1} = b_n - (n+1)(a_{n+1} - a_n)b \quad (8)$$

must be satisfied. From this recurrence relation the $\{b_n\}$ can be determined from a knowledge of the $\{a_n\}$, provided that an initial value, e.g. that of b_0, is specified. It is convenient to set $b_0 = 0$, and we do so. The double integral in Eq. (6) can now be evaluated, with the result

$$\int_{-\infty}^{\infty} dx_1 \int_{-\infty}^{\infty} du \exp[i(q-k)u] \langle \exp[iau\zeta'(x_1)] \rangle$$

$$= \frac{2\pi L_1}{(\omega/c)(\cos\theta_0 + \cos\theta_s)} f\left(\frac{\sin\theta_0 - \sin\theta_s}{\cos\theta_0 + \cos\theta_s}\right). \qquad (9)$$

The mean differential reflection coefficient thus is given in terms of the pdf of a_n,

$$\left\langle \frac{\partial R}{\partial \theta_s} \right\rangle = \frac{[1 + \cos(\theta_0 + \cos\theta_s)]^2}{\cos\theta_0(\cos\theta_0 + \cos\theta_s)^3} f\left(\frac{\sin\theta_0 - \sin\theta_s}{\cos\theta_0 + \cos\theta_s}\right). \qquad (10)$$

The change of variable $(\sin\theta_0 - \sin\theta_s)/(\cos\theta_0 + \cos\theta_s) = -\gamma$, allows us to write $f(\gamma)$ in terms of the mean differential reflection coefficient,

$$f(\gamma) = \frac{2}{1+\gamma^2} \frac{\cos\theta_0}{\cos\theta_0 + \gamma\sin\theta_0} \left\langle \frac{\partial R}{\partial \theta_s} \right\rangle (-\gamma, \theta_0), \qquad (11)$$

where $\langle \partial R/\partial\theta_s \rangle(\gamma, \theta_0)$ is the expression for $\langle \partial R/\partial\theta_s \rangle$ in which its dependence on θ_s has been replaced by its dependence on γ and θ through the use of the change of variable we have made.

If we seek to design a random surface that gives rise to a mean differential reflection coefficient that is a constant in the angular interval $-\theta_m < \theta_s < \theta_m$, and vanishes outside this interval,i.e. for which

$$\left\langle \frac{\partial R}{\partial \theta_s} \right\rangle = A\theta(\theta_s + \theta_m)\theta(\theta_m - \theta_s), \qquad (12)$$

where $\theta(z)$ is the Heaviside unit step function, it is found that the corresponding pdf $f(\gamma)$ is given by

$$f(\gamma) = \frac{2A}{1+\gamma^2} \frac{\cos\theta_0}{\cos\theta_0 + \gamma\sin\theta_0} \theta\left(\gamma + \tan\frac{\theta_m - \theta_0}{2}\right) \theta\left(\tan\frac{\theta_m + \theta_0}{2} - \gamma\right). \qquad (13)$$

The coefficient A in this expression is obtained by normalizing $f(\gamma)$ to unity. From this result for $f(\gamma)$ a long sequence of $\{a_n\}$ is generated by the rejection method [22], and the corresponding sequence of $\{b_n\}$ is obtained from Eq. (8). The surface profile function $\zeta(x_1)$ is then constructed on the basis of Eq. (7).

To determine whether the random surface generated in this fashion indeed produces the scattering pattern specified by Eq. (12), we proceed as follows. A large number N_p of realizations of the random surface is generated by the method just described, and for each realization the scattering problem is solved by, for example, a rigorous computer-based method [23] to yield the scattering amplitude $R(q|k)$. An arithmetic average of the N_p results for $|R(q|k)|^2$ obtained in this way yields the average $\langle |R(q|k)|^2 \rangle$ entering the expression for the mean differential

reflection coefficient given by Eq. (3). The computed result for $\langle \partial R / \partial \theta_s \rangle$ is then compared with the result given by Eq. (12).

Numerical results illustrating this approach to the design of one-dimensional random surfaces with specified scattering properties will be presented in this lecture, as well as a method for fabricating them on photoresist. Experimental results for the mean differential reflection coefficients measured in scattering from surfaces designed in the manner described will be also presented.

Extensions of the method described here for the design of one-dimensional randomly rough surfaces with specified scattering properties to the design of two-dimensional randomly rough surfaces with specified scattering properties will also be described, together with methods for fabricating them on photoresist. Experimental results for scattering from surfaces designed and fabricated by these methods will also be presented.

Bibliography

[1] J. C. Stover, *Optical Scattering* (SPIE, Bellingham WA, 1995).
[2] F. Grum and G. W. Luckey, Appl. Opt. **7**, 2295 (1968).
[3] H. P. Baltes, in *Inverse Scattering Problems in Optics*, ed. H. P. Baltes (Springer-Verlag, New York, 1980), pp. 1-13.
[4] C. N. Kurtz, J. Opt. Soc. Am. **62**, 982 (1972).
[5] C. N. Kurtz, H. O. Hoadley, and J. J. De Palma, J. Opt. Soc. Am. **63**, 1080 (1973).
[6] Y. Nakayama and M. Kato, Appl. Opt. **21**, 1410 (1982).
[7] M. Kowalczyk, J. Opt. Soc. Am. A**1**, 192 (1984).
[8] See, e.g. Thorlabs, Inc., Newton, New Jersey 07860-0366, U.S.A.
[9] Physical Optics Corp., Torrance, California 90501-1821, U.S.A.
[10] T. A. Leskova, A. A. Maradudin, I. V. Novikov, A. V. Shchegrov, and E. R. Méndez, Appl. Phys. Lett. **73**, 1943 (1998).
[11] E. R. Méndez, G. Martinez-Niconoff, A. A. Maradudin, and T. A. Leskova, SPIE **3426**, 2 (1998).
[12] A. A. Maradudin, I. Simonsen, T. A. Leskova, and E. R. Méndez, Opt. Lett. **24**, 1257 (1999).
[13] A. A. Maradudin, T. A. Leskova, E. R. Méndez, and A. V. Shchegrov, Physics of the Solid State **41**, 835 (1999).
[14] E. I. Chaikina, E. E. García-Guerrero, Zu-Han Gu, T. A. Leskova, A. A. Maradudin, E. R. Méndez, and A. V. Shchegrov, in *Frontiers of Laser Physics and Quantum Optics*, eds. Z. Xu, S. Xie, S. Y. Zhu, and M. O. Scully (Springer-Verlag, New York, 2000), pp. 225-259.
[15] I. Simonsen, T. A. Leskova, A. A. Maradudin, and E. R. Méndez, Waves in Random Media**11**, 529 (2001).
[16] E. R. Méndez, E. E. García-Guerrero, H. M. Escamilla, A. A. Maradudin, T. A. Leskova, and A. V. Shchegrov, Appl. Opt. **40**, 1098 (2001).

[17] E. R. Méndez, E. E. García-Guerrero, T. A. Leskova, A. A. Maradudin, J. Muñoz-Lopez, and I. Simonsen, Appl. Phys. Lett. **81**, 798 (2002).
[18] E. R. Méndez, E. E. García-Guerrero, T. A. Leskova, A. A. Maradudin, J. Muñoz-Lopez, and I. Simonsen, SPIE **4780**, 40 (2002).
[19] A. A. Maradudin, E. R. Méndez, and T. A. Leskova, Opt. Lett. **28**, 72 (2002).
[20] A. A. Maradudin, E. R. Méndez, and T. A. Leskova, SPIE **4780**, 51 (2002).
[21] T. A. Leskova, A. A. Maradudin, E. R. Méndez, and J. Muñoz-Lopez, in *Contemporary Mathematics*, ed. P. Kuchment (American Mathematical Society, Providence, R. I.) (to appear).
[22] W. H. Press, S. A. Teukolsky, W. T. Vetterling, and B. P. Flannery, *Numerical Recipes in Fortran, 2nd Edition* (Cambridge University Press, New York, 1992), pp. 281-282.
[23] A. A. Maradudin, T. Michel, A. R. McGurn, and E. R. Méndez, Ann. Phys. (N.Y.) **203**, 255 (1990).

Lateral surface superlattices: minibands, transport, and chaos

U. Rössler
Fakultät für Physik, Universität Regensburg, D-93040 Regensburg, Germany

The two-dimensional electron gas (2DEG), realized in semiconductor heterostructures and quantum wells, has become a model system for many different investigations. One field of research is based on applying modern semiconductor technologies, to impose a lateral periodic structure onto the 2DEG with periods a (now in the range of 100 nm) which are much smaller than the electron mean-free path l_{mfp} at low temperatures but comparable to the Fermi wavelength λ_F [1–3]. Thus, in a low-temperature transport experiment, the electrons can explore the periodic potential landscape without being scattered by impurities or phonons ($l_{\mathrm{mfp}} \ll a$). Considering at the same time that for the prevailing carrier densities $\lambda_F = 2\pi/k_F$ is comparable to a, the electrons in a lateral superlattice represent a model of a solid, but with lattice constants very much larger than the crystalline ones of a few Å. The characteristic energy spectrum of electrons in a periodic potential is a band structure, which due to the scaling of the lattice constant results here in minibands, with widths and gaps in the meV range. The demonstration of miniband formation has been one of the challenges of this system.

Experimental investigations of these systems preferentially employ magnetotransport measurements with the magnetic field applied perpendicular to the plane of the 2DES. With the magnetic length $l_B = \sqrt{\hbar/eB}$ a new scale is introduced

which can be tuned from the outside to study different regimes. If $l_B \ll a$, the periodic modulation becomes irrelevant and the electrons behave (up to small modifications) as the free 2D electrons in high magnetic field where the magnetoconductivity shows Shubnikov–de-Haas (SdH) oscillations. However, for magnetic fields with $l_B \simeq a$, the conductivity is significantly determined by the periodic structure, showing for $\lambda < a$ and strong potential modulation pronounced commensurability peaks [3], which are well described by classical [4] and quantum-mechanical [5, 6] transport simulations using the Kubo formula.

For even smaller magnetic fields in only moderately modulated systems and $\lambda_F \simeq a$, the electron motion can be described in the semiclassical picture which employs the formation of a band structure (with small gaps) and Fermi contours defining **k**-space orbits for electrons moving in the applied magnetic field. Within this picture, observed magnetotransport oscillations have been identified as fingerprints of a band structure in lateral surface superlattices [7].

In the classical regime, the 2DEG with periodic potential and perpendicular magnetic field represents a system with nonlinear dynamics. Depending on the relation between l_B, a, and the cyclotron radius $R_c = l_B^2 k_F$, the electrons move on (distorted) localized cyclotron orbits (for high magnetic field) but explore the hole space in chaotic orbits at lower fields. Commensurability peaks can be well understood as a result of this chaotic behavior by simulating magnetotransport with the classical Kubo formula [4]. In a quantum-mechanical picture the signatures of chaos are identified by level statistics [8–12].

One of the most striking properties of the electronic structure in a periodic potential in dependence on a magnetic field is the Hofstadter butterfly [13, 14]: depending on the magnetic flux threading a unit cell the electronic spectrum shows a fractal structure of bands and gaps which after long efforts has finally been verified in magnetotransport experiments [15].

Besides by electrostatic modulation investigations have been carried out also for lateral surface superlattices with magnetostatic modulation [16, 17], with a periodic structure created by superconducting islands [18], and for 2D hole systems [19].

Bibliography

[1] D. Weiss, C. Zhang, R. R. Gerhardts, K. von Klitzing, G. Weimann, Phys. Rev. B **39**, 13020 (1989).

[2] R. W. Winkler, J. P. Kotthaus, K. Ploog, Phys. Rev. Lett. **62**, 1177 (1989).

[3] D. Weiss, M. L. Roukes, A. Menschig, P. Grambow, K. von Klitzing, G. Weimann, Phys. Rev. Lett. **66**, 2790 (1991).

[4] R. Fleischmann, T. Geisel, R. Ketzmerick, Phys. Rev. Lett. **68**, 1367 (1992).

[5] H. Silberbauer and U. Rössler, Phys. Rev. B **50**, 11911 (1994).

[6] M. Langenbuch, M. Suhrke, U. Rössler, Europhys. Lett. **61**, 520 (2003).
[7] C. Albrecht, J. H. Smet, D. Weiss, K. von Klitzing, R. Hennig, M. Langenbuch, M. Suhrke, U. Rössler, V. Umansky, H. Schweizer, Phys. Rev. Lett. **83** 2234 (1999).
[8] H. Silberbauer, P. Rotter, M. Suhrke, and U. Rössler, Semicond. Sci. Technol. **9**, 1906 (1994).
[9] H. Silberbauer, P. Rotter, U. Rössler, and M. Suhrke, Europhys. Lett. **31**, 393 (1995).
[10] O. Steffens, M. Suhrke, and P. Rotter, Phys. Rev. B **55**, 4486 (1997).
[11] M. Suhrke and P. Rotter, in: *Theory of transport properties of semiconductor nanostructures*, ed.: E. Schöll (Chapman and Hall, London, 1998), p. 249.
[12] O. Steffens, T. Schlösser. P. Rotter, K. Ennslin, M. Suhrke, J. P. Kotthaus, U. Rössler, M. Holland, J. Phys.: Cond. Matter **10** 3859 (1998).
[13] R. D. Hofstadter, Phys. Rev. B**14**, 2239 (1976).
[14] U. Rössler, M. Suhrke, in:*Advances in Solid State Physics* **40**, ed. by B. Kramer (Vieweg, Braunschweig 2000) p. 35.
[15] C. Albrecht, J. H. Smet, K. von Klitzing, D. Weiss, V. Umansky, H. Schweitzer, Phys. Rev. Lett. **86**, 147 (2001).
[16] P. D. Ye, D. Weiss, K. von Klitzing, K. Eberl, H. Nickel, Appl. Phys. Lett. **67**, 1441 (1995).
[17] R. Hennig, M. Suhrke, Phys. Rev. B **60**, 11535 (1999).
[18] J. Eroms, M. Tolkiehn, D. Weiss, U. Rössler, J. DeBoeck, G. Borghs, Europhys. Lett. **58**, 569 (2002).
[19] M. Zitzelsperger, R. Onderka, M. Suhrke, U. Rössler, D. Weiss, W. Wegscheider, R. Winkler, Y. Hirayama, K. Muraki, Europhys. Lett. **61**, 382 (2003).

Разбавленные ферромагнитные полупроводники. Теория и эксперимент

К. А. Кикоин
Университет Бен-Гурион, Беер-Шева, Израиль

Разбавленные магнитные полупроводники (РМП) — это полупроводниковые соединения группы A_3B_5, в которых часть атомов одной из подрешеток замещена примесями переходных или редкоземельных металлов. При достаточно высокой концентрации магнитных ионов в сплаве возникает ферромагнитный порядок. Если температура Кюри T_C достаточно высока, то появление такого материала чрезвычайно расширяет возможности современной микроэлектроники и спинтроники. Марганец оказался наиболее подходящей магнитной примесью благодаря своей высокой растворимости и диффузионной

способности. К настоящему времени получены РМП с $T_C \sim 160$ K на основе p-($Ga_{1-x}Mn_x$)As. В широкощелевых материалах p-(Ga,Mn)P, а также p- и n-(Ga,Mn)N ферромагнетизм обнаружен и при температурах, превышающих комнатную.

На первый взгляд возникновение магнитного порядка в этих системах представляется вполне естественным следствием наличия магнитного момента у ионов марганца. Если найдена технологическая возможность растворять эти ионы в полупроводниках в достаточной концентрации без кластеризации примесей или образования преципитатов других фаз, то примесный магнетизм возникнет в соответствии с известными сценариями теории неупорядоченных магнетиков [1]: сначала образуется перколяционная сетка магнитных моментов, связанных обменным взаимодействием, а при дальнейшем повышении концентрации Mn возникает эффективное молекулярное поле, обеспечивающее дальний магнитный порядок.

Однако, *ферромагнитный* характер магнитного упорядочения в легированных полупроводниках представляет определенный вызов для теории. Во-первых, прямое обменное взаимодействие в разбавленных магнитных сплавах слишком мало, чтобы обеспечить такие высокие T_C, а большинство известных механизмов косвенного обмена благоприятствует *антиферромагнитому* упорядочению. Во-вторых, ион марганца как примесь замещения в полупроводниках A_3B_5 является довольно сложным дефектом, который не только привносит в матрицу магнитный момент, но и преобразует электронный спектр ближайшего окружения примеси [2, 3].

Простейший (и наиболее популярный) феноменологический подход [4] игнорирует эти проблемы. В качестве исходного взаимодействия между локальным спином магнитной примеси и электронами (дырками) в валентной зоне берется sd-обмен Вонсовского–Зинера. Он порождает косвенное взаимодействия Рудермана-Киттеля между магнитными ионами, которому приписывается ферромагнитный знак. Температура Кюри вычисляется в приближении среднего поля для примесного магнетизма [5]. Более реалистический подход основан на расчете электронного спектра РМП с помощью численного метода расширенных кластеров, в котором взаимодействие магнитного иона с ближайшим окружением учитывается максимально точно, затем строится периодическая сверхрешетка и делается зонный расчет спин-поляризованной электронной структуры, иногда с учетом локальных поправок типа когерентного потенциала [6]. Этот подход позволяет вычислить T_C и обладает определенной предсказательной силой, но на его основе довольно трудно определить, как именно устроен механизм обменного взаимодействия между ионами марганца .

Мы поставили себе задачу вывести межпримесное ферромагнитное взаимодействие в РМП *микроскопически*, основываясь на детальном знании электронной структуры изолированной примеси Mn в матрицах A_3B_5 [3]. Оказалось [7], что в кристаллах p-типа это взаимодействие не сводится ни к одному из известных типов непрямого обмена, хотя и напоминает механизм двойного обмена, предложеный Зинером полвека тому назад [8]. В системе n-(Ga,Mn)N зинеровский обмен реализуется почти в своем классическом виде. Полученные формулы для концентрационной зависимости T_C воспроизводят экспериментальные данные для p-(Ga,Mn)As. Для других систем зависимость T_C от концентрации носителей еще экспериментально не установлена, однако теория позволяет получить T_C выше комнатной температуры при разумных значениях параметров модели.

Изовалентные примеси переходных металлов (Tr), замещающие катионы Ga в решетке цинковой обманки, должны быть трехвалентным ионами. Это значит, что атомы Tr($3d^n4s^2$) ионизуются до трехвалентного состояния $Tr^{3+}(3d^{n-1})$. Марганец, Mn($3d^54s^2$), является исключением из общего правила, поскольку полузаполненная 3d-оболочка этого элемента аномально устойчива по правилу Хунда. В большинстве случаев [p-(Ga,Mn)As, p-(Ga,Mn)P] энергетически выгодно образование примесного «кластера» $Mn^{3+}(3d^5p)$ вместо иона $Mn^{3+}(3d^4)$. Здесь символ p означает локальное дырочное состояние, построенное как суперпозиция состояний валентной зоны матрицы. В результате эффективный обмен между соседними магнитными ионами в этой матрице осуществляется в меру перекрытия кластеров. Микроскопическая теория такого обмена [7] строится на основе двухпримесной модели Андерсона [9], обобщенной на случай полупроводниковой матрицы и учитывающей реальную электронную структуру Mn. В соответствии с этой теорией энергетически предпочтительным оказывается своеобразный вариант ферромагнитного двойного обмена, когда соседние ионы Mn обмениваются парой электронов, причем перескоки *без переворота спина* осуществляются через незаполненные p-состояния в районе потолка валентной зоны. В системе n-(Ga,Mn)N с аномально широкой энергетической щелью примеси марганца оказываются в состоянии $Mn^{3+}(3d^4)$ и образуют примесную зону глубоко в запрещенной зоне. Примесная зона частично заполнена, и это означает, что часть ионов находится в состоянии $Mn^{2+}(3d^5)$. Таким образом реализуется случай «промежуточной валентности», рассмотренный в классической работе Зинера [8]. Двойной обмен Зинера в примесной зоне дает более высокие T_C, чем в p-(Ga,Mn)As, в силу большой плотности состояний.

Теория позволяет дать количественное описание зависимости $T_C(x)$, наблюдаемой в эксперименте (см., напр. [10]), и указывает на существенные

различия между магнитными полупроводниками p- и n-типа. Кроме того, она может быть обобщена на случаи пониженной размерности (гетероструктуры, квантовые ямы), существенные для многочисленных практических приложений.

Литература

[1] I. Ya. Korenblit, E. F. Shender, and B. I. Shklovskii, Phys. Lett. **46**A, 275 (1973); И. Я. Коренблит, Е. Ф. Шендер, УФН **126**, 233 (1978).

[2] A. Zunger, in *Solid State Physics*, Ed. by H. Ehrenreich and D. Turnbull (Academic, Orlando), Vol. 39, 276 (1986).

[3] K. A. Kikoin and V. N. Fleurov, *Transition Metal Impurities in Semiconductors* (World Scientific, Singapore), (1994).

[4] T. Dietl, H. Ohno, and F. Matsukara, Phys. Rev. B **63**, 2034 (2001); **66**, 033203 (2002).

[5] А. А. Абрикосов, Л. П. Горьков, ЖЭТФ **44**, 2230 (1962).

[6] E. Kulatov *et al*, Phys. Rev. B **66**, 045203 (2002); K. Sato, P. H. Dederichs and H. Katayama-Yoshida, Europhys. Lett. **61**, 403 (2003).

[7] P. M. Krstajic, V. A. Ivanov, F. M. Peeters, V. Fleurov, and K. Kikoin, Europhys. Lett. **61**, 235 (2003); arXiv:cond-mat/0311525.

[8] C. Zener, Phys. Rev. **82**, 403 (1951).

[9] S. Alexander and P. W. Anderson, Phys. Rev. **133**, A1594 (1964).

[10] K. M. Yu, *et al*, Appl. Phys. Lett. **81**, 5 (2002); K. W. Edmonds, *et al*, Appl. Phys. Lett. **81**, 3010 (2002); T. Graf, *et al*, Appl. Phys. Lett. **81**, 5159 (2002).

Temperature scaling in the integer quantum hall effect regime: experiments

B. Pődör

Hungarian Academy of Sciences, Research Institute for Technical Physics and Materials Science, Budapest, Hungary and Budapest Polytechnic, Kandó Kálmán Faculty of Electrical Engineering, Institute of Microelectronics and Technology, Budapest, Hungary

A concise review of temperature scaling experiments in the plateau-to-plateau transitions on the integral quantum Hall effect is presented. Some new results on temperature scaling in the plateau-to-plateau transitions as well as on the $i = 1$ plateau-to-insulating phase transitions in two-dimensional electron gas in $In_{0.53}Ga_{0.47}As/InP$ heterostructures are also presented.

1. Introduction

The transport properties of two-dimensional electron gas (2DEG) continue to attract much interest both experimentally and theoretically. Recently there has been an upsurge of interest in the scaling behaviour of transport coefficients in the quantum Hall effect in connection with the question of universality of the scaling exponent.

The steps connecting the quantum Hall plateaus in ρ_{xy} as well as the peaks of the longitudinal resistivity ρ_{xx} become sharper with decreasing temperature. The scaling theory of the integer quantum Hall effect (IQHE) predicts [1] that a universal critical exponent $\varkappa$ describes the temperature dependence of the linewidth of the ρ_{xx} peaks and the maximum slope of ρ_{xy} between the plateaus

$$\Delta B \sim T^{\varkappa} \text{ and } (d\rho_{xy}/dB)_{\max} \sim T^{-\varkappa}.$$

These relationships follow from the scaling theory result that ρ_{xx} and ρ_{xy} both depend on the temperature and magnetic field only through the single variable $(B-B_c)T^{-\varkappa}$ [2, 3]. The exponent $\varkappa$ is given by the ratio $\varkappa = p/2\alpha$, where p is the inelastic scattering length exponent and α is the localization length exponent. The localization length ξ of the levels near the Fermi energy diverges like a universal power law

$$\xi = \xi_0 \mid B - B_c \mid^{-\alpha}$$

here B_c is the critical magnetic field corresponding to the singular point in the free electron spectrum of the Landau level at $T = 0$ [1]. At finite but low temperature the characterisitc length is the unelastic scattering length given by

$$L_{in}(T) \sim T^{-p/2}.$$

In a number of experiments, [4–12] (for reviews see [13–15]) it was found that the width of the peaks in ρ_{xx} shrinks as a power law $T^{\varkappa}$, as stipulated by the relevant theory. Early experiments on InGaAs/InP heterostructures [4, 6], and later on other material systems resulted in $\varkappa = 0.42 \pm 0.04$, subsequently considered as a universal value, while other experiments [5, 7–9] mainly on GaAlAs/GaAs heterostructures show that the scaling exponent $\varkappa$ depends on both density and type of doping and is also different for transitions between different Landau levels, yielding $0.2 \leq \varkappa \leq 1.0$. The main difference between these two material systems is in the type and character of the dominant electron scattering mechanism. In the GaAs based system longer range potential fluctuations prevail, while in the InGaAs/InP heterojunction the electron scattering is dominated by alloy disorder, which approximately can be described by uncorrelated δ-function potentials also

used in deriving the predictions of the scaling theory. Further on there are also some experiments which even claim the absence of scaling in the transitions between the IQHE plateaus [16]. Thus the apparent power law with a possible non-universal exponent $\varkappa$ is still a controversial issue.

In the past years the experiments extended the reach of scaling studies to the transition from the quantum Hall (QH) state to the insulating phase (IP) below the $i = 1$ quantum Hall plateau in the range of fractional filling of the lowest Landau level, the IP being supposed to be a Hall insulator [17–24]. Striking similarities in the scaling behaviour in the transitions between the different QH states were observed [18, 19], hinting the same universality class for both types of transitions [19–23]. However, also for the $i = 1$ quantum Hall liquid (QHL)-to IP transition various values of the temperature scaling exponent ranging from 0.4 to 0.7 have been reported [19–23].

Here I present some results of a new study of the temperature scaling exponents for the low Landau index integer quantum Hall effect (IQHE) plateau-to-plateau as well as for the $i = 1$ plateau-to-insulating phase transitions in 2DEG in $In_{0.53}Ga_{0.47}As/InP$ modulation-doped heterostructures. Preliminary results have already been published in [25], and a more detailed account is in preparation [26].

2. Samples and experiments

The samples used in this study were liquid phase epitaxially grown modulation-doped $In_{0.53}Ga_{0.47}As/InP$ heterostructures [27-30]. The 2DEG density and mobility were $(0.3-4) \times 10^{11}$ cm^{-2} and $(2-6) \times 10^4$ cm^2/Vs respectively. The strength of the disorder potential in our samples was assessed from the broadening of the Landau levels and from the ratio of the transport scatterig time to the quantum scattering time, τ_t/τ_q, deduced from the decay of the amplitude of the Shubnikov-de Haas oscillations in low magnetic fields [29, 31, 32]. The values of τ_t/τ_q increased with increasing 2DEG concentration. Typical values were ~ 1.5, 2 to 3, and 6 to 8 respectively for concentrations of $(4-5) \times 10^{10}$, $(1-2) \times 10^{11}$, and $(3-4) \times 10^{11}$ cm^{-2} respectively, reflecting the dominant nature of small-angle scattering, i.e. of alloy disorder scattering and of scattering on interface irregularities at low 2DEG concentrations [31, 32].

Magnetotransport measurements were carried out on photolithographically defined double cross Hall bars in the temperature range from 40 mK to 4.2 K in a superconducting magnet up to about 6 T, and also in a resistive magnet up to 20 T. Persistent photoconductivity was used to control the 2DEG density. Both conventional dc and low-frequency lock-in techniques were used. For the plateau-to-plateau transitions in the IQHE the scaling exponents were extracted from the

temperature dependence of the linewidth of the ρ_{xx} peaks and from the maximum slope of ρ_{xy} between plateaus, i.e. $(\Delta B)^{-1} \sim T^{-\varkappa}$ and $(d\rho_{xy}/dB)_{\max} \sim T^{-\varkappa}$. For the QHL $(i = 1)$ plateau-to-IP transition the scaling exponent was determined using the appropriate scaling relationships.

3. Results

In Fig. 1 the Hall resistivity ρ_{xy} and its derivative with respect to the magnetic field $d\rho_{xy}/dB$ are shown for a sample with $n_s = 1.20 \times 10^{11}$ cm^{-2} and $\mu = 3 \times 10^4$ cm^2/Vs as a function of the magnetic field at several temperatures. The spin splitting of the first Landau level $(N = 1)$ is not resolved in this particular sample due to the relatively large broadening of the Landau levels as indicated also by the low mobility. The maxima of $d\rho_{xy}/dB$ clearly increase with decreasing temperature.

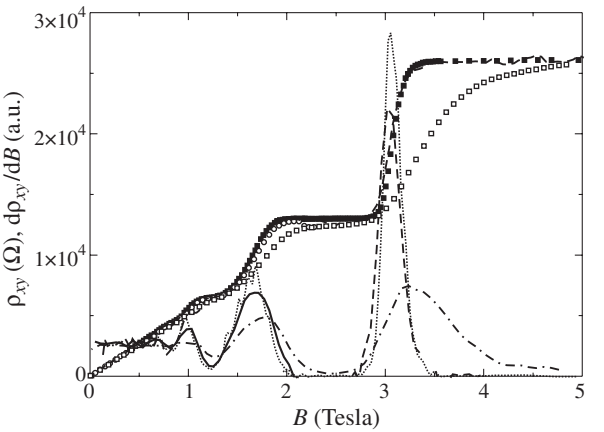

Figure 1. Hall resistivity ρ_{xy} and its derivative with respect to the magnetic field $d\rho_{xy}/dB$ at temperatures 0.75, 0.81, 1.53, and 4.2 K for a sample with $n_s = 1.20 \times 10^{11}$ cm^{-2} and $\mu = 3 \times 10^4$ cm^2/Vs.

Fig. 2 shows $(d\rho_{xy}/dB)_{\max}$ for Landau levels $N = 0$ ($i = 1$ to 2 transition) and $N = 1$ ($i = 2$ to 4 transition), and the reciprocal halfwidth $(\Delta B)^{-1}$ of the ρ_{xx} peak $N = 0$ in function of the temperature. The temperature scaling behaviour is convincingly demonstrated. In this sample for the $i = 1$ to 2 transition the temperature dependence of the maximum slope of ρ_{xy} resulted in $\varkappa = 0.75 \pm 0.12$ while the width of the ρ_{xx} peak gave $\varkappa = 0.63 \pm 0.08$. According to [6] for spin degenerate levels the scaling exponent is half of that of the non-degenerate levels, i.e. $\varkappa/2$. In this sample the experimental value for the $N = 1$ level was found to

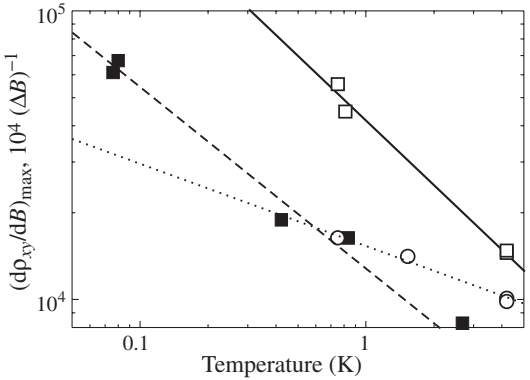

Figure 2. Maxima of $d\rho_{xy}/dB$ for $N = 0$ (squares) and 1 (circles), and reciprocal halfwidth of ρ_{xx} for $N = 0$ (filled squares) as function of the temperature.

be $\varkappa/2 = 0.29 \pm 0.03$, which is close to but somewhat less than the half of the value derived for the $N = 0$ level.

In the analysis of data taken in other similar samples transitions corresponding to $i = 1$ to 2 ($N = 0$ spin-down Landau level), to $i = 2$ to 4 ($N = 1$, no spin splitting) and $i = 2$ to 3 and 3 to 4 ($N = 1$ spin-splitted levels), and in a few cases also to $i = 4$ to 6 ($N = 2$, no spin splitting) were evaluated.

The values of the $\varkappa$ scaling exponent for the plateau-to-plateau transitions involving the $N = 0$ and the spin degenerate $N = 1$ Landau levels were found to lie consistently in the range of 0.6 to 0.8, however the estimated error was rather large, usually $\pm$ (0.1 to 0.2). In some samples the $i = 2$ to 3 and 3 to 4 transitions in the $N = 1$ level were partially resolved. In these cases the scaling exponent $\varkappa$ for the separate spin-up and spin-down levels were in the range from 0.45 to 0.55, i.e. smaller than the values obtained for the $N = 0$ level, but still greater than the presumed universal value [1, 4]. Finally the $i = 4$ to 6 transition in the spin degenerate $N = 2$ Landau level yielded values for $\varkappa/2$ in the range from 0.22 to 0.33.

Beyond the $N = 0$ Landau level with increasing magnetic field an insulating phase emerges [17, 19, 30], the onset of which is shifted toward higher fractional filling factors $\nu = en_s/hB$, i.e. lower magnetic field with increasing disorder in the 2DEG. For a sample with high disorder (and very low 2DEG concentration) Fig. 3 shows the QHL ($i = 1$)-to-IP transition. The transition from the quantum Hall liquid to the insulating phase occurring at $B = B_c$ is determined by the crossing points of the $\rho_{xx}(B)$ curves measured at different temperatures. At this point the direction of the temperature dependence of the resistivity changes sign. For

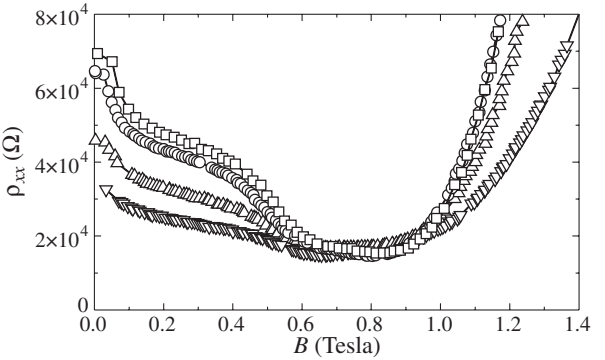

Figure 3. QHL ($i = 1$)-to-IP transition with increasing magnetic field in a sample with strong disorder ($n_s = 2.7 \times 10^{10}$ cm^{-2}). Down triangles — 800 mK, up triangles — 400 mK, circles — 200 mK, squares — 100 mK.

$B < B_c$ the longitudinal resistivity decreases with decreasing temperature (metallic behaviour in the QHL), for $B > B_c$ the longitudinal resistivity increases with decreasing temperature (insulating behaviour in the IP). Supposing the validity of the scaling law, $\rho_{xx}(B) = f(\mid B - B_c \mid T^{-\varkappa})$, the scaling exponent is obtained from $(d\rho_{xx}/dB)|_{B=B_c} \sim T^{-\varkappa}$. For the correct value of $\varkappa$ the ρ_{xx} curves measured at different temperatures, when plotted in function of $\mid B - B_c \mid T^{-\varkappa}$ collapse into

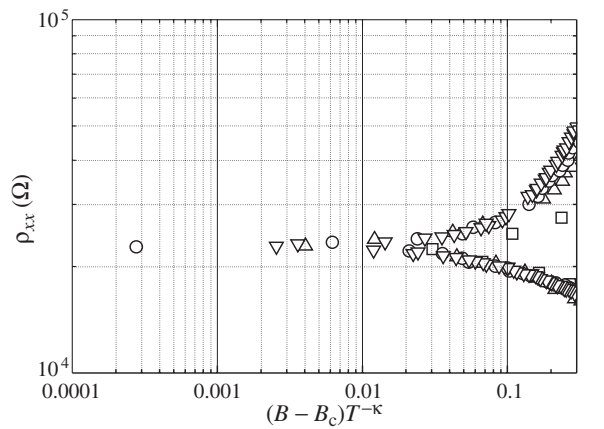

Figure 4. Longitudinal resistivity ρ_{xx} versus $\mid B - B_c \mid T^{-\varkappa}$ with the scaling exponent determined as $\varkappa = 0.77 \pm 0.08$ to collapse the data points at different temperatures to a single curve.

one single curve with two branches, one branch for $B < B_c$, the other one for $B > B_c$, as shown in Fig. 4, with $\varkappa = 0.77 \pm 0.08$ for this particular sample.

In other samples too the values of the $\varkappa$ exponent for the QHL $(i = 1)$-to-IP transition were also found in the range of 0.6 to 0.8, with an estimated error of about ± 0.1. The critical filling factor $\nu_c = en_s/hB_c$ for this transition was in the range from about 0.5 to 1, and the critical value of ρ_{xx} at the transition amounted to $\rho_c = (0.8{-}1.3)h/e^2$.

4. Discussion

The experimentally determined scaling exponent for the $i = 1$ to 2 plateau-to-plateau transition and for the $i = 1$ Hall plateau-to-insulating phase transition is the same within experimentally error. This indicates that both transitions belong to the same universality class, in accordance with the literature. However the value of the $\varkappa$ exponent found in our liquid phase epitaxially grown InGaAs/InP samples for these two transitions is significantly greater than the value of ~ 0.42 hitherto considered to be universal. However the value of $\varkappa = 0.6{-}0.8$ for the QHL $(i = 1)$-to-IP transition found here agrees with the values found recently for the same transition in vapour phase epitaxial InGaAs/InP heterostructures [21, 23] and also in Si/SiGe heterostructures [20].

The larger values of the scaling exponent for the plateau-to-plateau transition in the low index ($N = 0$, 1 and 2) Landau levels found in this work, especially their deviation from the presumed universal value are similar to that found in several other works [5, 8, 33]. As already mentioned above the scaling exponent can be expressed as $\varkappa = p/2\alpha$ [1, 4, 5, 13]. The numerically calculated value of the localization length exponent (which is predicted to be universal [1]) is $\alpha = 2.35 \pm 0.03$ in the lowest Landau level for a potential with short-range correlations [13, 34]. For zero magnetic field $p = 1$ in the "dirty metal limit" and $p = 2$ for "clean samples" in the Fermi liquid theory [33]. The value of $\varkappa = 0.42$, considered universal in the literature, is in accordance with $p = 2$. On the other hand the experimental values of $\varkappa$ found in this work would indicate larger values of the inelastic scattering rate p in the range from 2.8 to 3.7, at least for the InGaAs/InP system with relatively large disorder studied here. Our conclusions concerning the larger values of the p exponent are in accordance among others with the results obtained in the AlGaAs/GaAs heterostructures [5, 33], where on the basis of similar p values it was stated that the actual value of p can be substantially larger in high magnetic fields compared to the theoretical zero-magnetic-field results.

5. Conclusions

We have studied the scaling behaviour of the quantum Hall plateau $(i = 1)$-to-insulating phase transition and of the transitions between the low index quantum Hall plateaus in 2DEG in InGaAs/InP heterostructures.

The scaling exponent for the transition from the first quantum Hall plateau to the insulating phase (supposed Hall insulator) was found equal to that for the quantum Hall plateau-to-plateau transition in the same material system, i.e. $\varkappa \approx 0.6-0.8$. This value of the scaling exponent is significantly greater than the value of $\varkappa \approx 0.42$, considered up to now universal in the literature. The experimental results have been interpreted by considering the enhanced values of the inelastic scattering rate exponent.

Acknowledgements

The contribution of Dr. Gy. Kovács, Dr. G. Remenyi, and Dr. I. G. Savel'ev to the results of this work are gratefully acknowledged. The samples used were grown by Dr. S. V. Novikov. This research was supported in part by a grant from the (Hungarian) National Research Fund (OTKA) project No. 31763. The high magnetic field measurements were performed at the CNRS/Max-Planck-Institut Grenoble High Magnetic Field Laboratory under projects No. SE1295, SE3196 and SE2198.

Bibliography

[1] A. M. M. Pruisken, Phys. Rev. Lett. **61**, 1297 (1988).
[2] A. M. M. Pruisken, Nucl. Phys. B **285**, 719 (1987) and **290**, 61 (1987).
[3] A. M. M. Pruisken, in: *The Quantum Hall Effect*, Ed. R. E. Prange and S. M. Girvin, 2nd edition, (Springer Verlag, Berlin), (1990).
[4] H. P. Wei, D. C. Tsui, M. A. Palaanen, and A. M. M. Pruisken, Phys. Rev. Lett. **61**, 1294 (1988).
[5] S. Koch, R. J. Haug, K. v. Klitzing, and K. Ploog, Phys. Rev. B **43**, 6828 (1991).
[6] S. W. Wang, H. P. Wei, L. W. Engel, D. C. Tsui, and A. M. M. Pruisken, Phys. Rev. B **48**, 11416 (1993).
[7] K.-H. Yoo, H. C. Kwon, and J. C. Park, Solid State Comm. **92**, 821 (1994).
[8] F. W. Van Keuls, H. W. Jiang, and A. J. Dahm, Czech. J. Phys. **46**(Suppl 5), 2467 (1996).
[9] R. Meisels, F. Kuchar, W. Belitsch, and B. Kramer, Microelectronic Engineering **47**, 23 (1999).
[10] J. Jaroszynski, G. Karczewski, J. Wrobel, T. Andrearczyk, A. Strycharczuk, T. Wojtowicz, G. Grabecki, E. Papis, E. Kaminska, A. Piotrowska, and T. Dietl, Physica E **6**, 790 (2000).
[11] F. Kuchar, R. Meisels, K. Dybko, and B. Kramer, Europhys. Lett. **49**, 480 (2000).

[12] F. Hohls, U. Zeitler, R. J. Haug, R. Meisels, K. Dybko, and F. Kuchar, Physica E **16**, 10 (2003).
[13] B. Huckestein, Rev. Mod. Phys. **67**, 357 (1995).
[14] S. L. Sondhi, S. M. Girvin, J. P. Carini, and D. Shahar, Rev. Mod. Phys. **69**, 315 (1997).
[15] K. Yang, D. Shahar, R. N. Bhatt, D. C. Tsui, and M. Shayegan, J. Phys. Cond. Matter **12**, 5343 (2000).
[16] N. Q. Balaban, U. Meirav, and I. Bar-Joseph, Phys. Rev. Lett. **81**, 4967 (1998).
[17] D. Shahar, D. C. Tsui, M. Shayegan, R. N. Bhatt, and J. E. Cunningham, Phys. Rev. Lett. **74**, 4511 (1995).
[18] D. Shahar, D. C. Tsui, M. Shayegan, E. Shimshoni, and S. L. Sondhi, Phys. Rev. Lett. **79**, 479 (1997).
[19] W. Pan, D. Shahar, D. C. Tsui, H. P. Wei, and M. Razeghi, Phys. Rev. B **55**, 15431 (1997).
[20] R. B. Dunford, N. Griffin, M. Pepper, P. J. Phillips, and T. E. Whall, Physica E **6**, 297 (2000).
[21] R. T. F. van Schaijk, A. de Visser, S. M. Olshthoorn, H. P. Wei, and A. M. M. Pruisken, Phys. Rev. Lett. **84**, 1567 (2000).
[22] R. B. Dunford, N. Griffin, P. J. Phillips, and T. E. Whall, Physica B **298**, 496 (2001).
[23] D. T. N. de Lang, L. Ponomarenko, A. de Visser, C. Possanzini, S. M. Ohlstoornn, and A. M. M. Pruisken, Physica E **12**, 666 (2002).
[24] B. Pődör, Gy. Kovács, G. Remenyi, and I. G. Savel'ev, in: *Proc. 11th Int. Workshop on Physics of Semiconductor Devices*, New Delhi, 2001, Eds. V. Kumar and P. K. Basu, Vol. 1, Allied Publishers, New Delhi, 2001, p. 298.
[25] B. Pődör, Gy. Kovács, G. Remenyi, and I. G. Savel'ev, in: *Proc. 12th Int. Workshop on Physics of Semiconductor Devices*, Madras, 2003, Ed. K. N. Bhat and A. DasGupta, Vol. 2, Narosa Publishing House, New Delhi, 2003, p. 1163.
[26] B. Pődör, Gy. Kovács, G. Remenyi, I. G. Savel'ev, and S. V. Novikov, to be published.
[27] L. V. Golubev, A. M. Kreshchuk, S. V. Novikov, T. A. Polyanskaya, I. G. Savel'ev, and I. I. Saidashev, Fiz. Tekh. Poluprovodn. **22**, 1948 (1989).
[28] V. V. Vorob'eva, M. V. Egorova, A. M. Kreshchuk, S. V. Novikov, I. G. Savel'ev, and I. I. Saidashev, Pis'ma Zh. Tekh. Fiz. **15**(11), 73 (1989).
[29] I. G. Savel'ev, A. M. Kreshchuk, S. V. Novikov, A. Ya. Shik, G. Remenyi, Gy. Kovács, B. Pődör, and G. Gombos, J. Phys. Cond. Matter **8**, 9025 (1996).
[30] B. Pődör, Gy. Kovacs, G. Remenyi, I. G. Savel'ev, and S. V. Novikov, Neorganicheskie Materialy **37**, 530 (2001).
[31] S. D. Bystrov, A. M. Kreshchuk, S. V. Novikov, T. A. Polyanskaya, and I. G. Savel'ev, Fiz. Tekh. Poluprovodn. **27**, 645 (1993).
[32] B. Pődör, S. V. Novikov, I. G. Savel'ev, and G. Gombos, Acta Physica Hungarica **71**, 147 (1994).
[33] S. Koch, R. J. Haug, K. v. Klitzing, and K. Ploog, Phys. Rev. Lett. **67**, 883 (1991).
[34] B. Huckestein and B. Kramer, Phys. Rev. Lett. **64**, 1437 (1990).

Осцилляции нелинейного магнитосопротивления высокоподвижных двумерных систем в неквантующих магнитных полях

В. А. Волков
Институт радиотехники и электроники РАН, Москва, Россия

Недавно начались тщательные исследования магнитотранспорта в высококачественных двумерных (2D) полупроводниковых электронных системах с подвижностями $\mu \sim (10^6 - 10^7)$ см^2/Вс в нелинейном режиме по внешнему электрическому полю, постоянному или переменному. В области относительно слабых магнитных полей B, которые сильны в классическом смысле ($\mu B \gg 1$), но слабее тех, в которых начинаются шубниковские осцилляции, при температуре $T \sim 1$ K обнаружен ряд замечательных явлений, включая осцилляции диагонального сопротивления при изменении величины тока, магнитного поля или частоты падающей на образец СВЧ волны.

В [1] обнаружены осцилляции магнитосопротивления при пропускании через двумерную систему в структуре GaAs-$Al_xGa_{1-x}As$ достаточно сильного постоянного тока I, см. рис. 1. Осцилляции были периодичны по величине I/B и связывались с зинеровским туннелированием между «наклоненными»

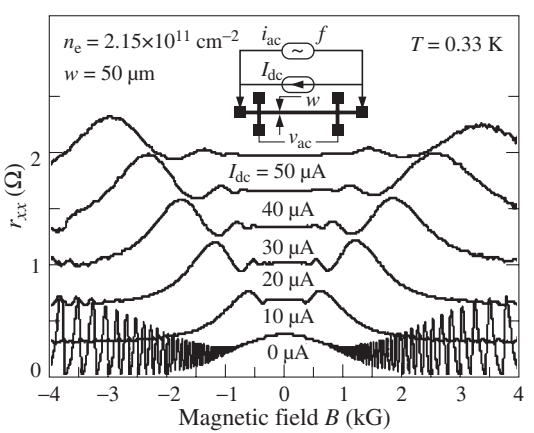

Рис. 1.

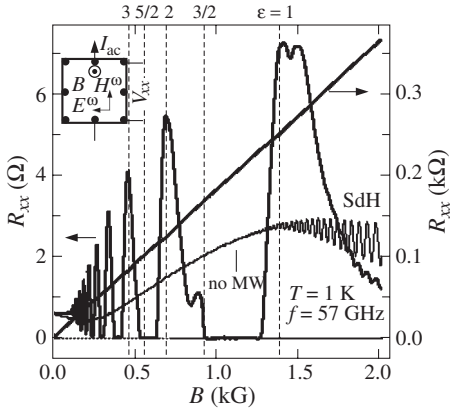

Рис. 2.

уровнями Ландау при рассеянии электронов на дефектах специального вида.

В подобной системе обнаружены [2] гигантские периодические по $1/B$ осцилляции статического магнитосопротивления в поле сильной СВЧ волны, но в линейном режиме по постоянному тянущему электрическому полю. Период осцилляций определялся целой частью отношения частоты волны к

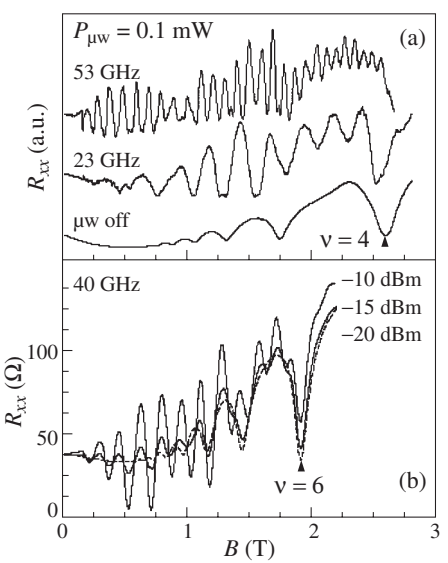

Рис. 3.

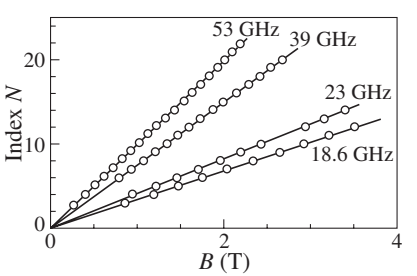

Рис. 4.

циклотронной частоте. При увеличении подвижности осцилляции усиливались с ростом мощности падающей волны, и при низких температурах сопротивление (для холловских образцов) или проводимость (для корбиновских образцов) исчезали [3, 4] в конечных интервалах магнитного поля, рис. 2. Реализация таких «бездиссипативных состояний» вызвала лавину теоретических работ. Предложенные в литературе сценарии позволяют качественно понять ряд важных особенностей обсуждаемых эффектов, но удовлетворительное объяснение в настоящее время отсутствует.

В конце 2003 г. в аналогичной системе обнаружен [5] еще один тип осцилляций магнитосопротивления, индуцированных СВЧ-излучением, рис. 3, и периодических по B, рис. 4, который объяснен возбуждением краевых магнитоплазмонов.

Доклад посвящен обзору полученных в этой области экспериментальных результатов и попыток их теоретического осмысления. Работа поддержана грантами РФФИ и ОФН РАН.

Литература

[1] C. L. Yang *et al*, Phys. Rev. Lett. **89**, 076801 (2002).
[2] M. A. Zudov *et al*, Phys. Rev. B **64**, 201311 (2001).
[3] R. G. Mani *et al*, Nature **420**, 646 (2002).
[4] M. A. Zudov *et al*, Phys. Rev. Lett. **90**, 46807 (2003).
[5] I. V. Kukushkin *et al*, arXiv: cond-mat/0312285.

Puzzles of low-temperature electron dephasing

V. I. Kozub
Ioffe Physico-Technical Institute of RAS, St. Petersburg, Russia

As early as in 1984, studying weak localization correction to the conductivity of In_2O_{3-x} films Ovadyahu [1] has found a puzzling behavior of the electron dephasing time τ_φ as a function of the static disorder. Namely, for a given temperature τ_φ^{-1} was scaled with a sample conductivity. This result contradicts the naive considerations that the disorder should lead to an increase of any scattering rate. While the similar behavior was predicted by Schmid [2] for electron-phonon scattering in dirty metals, in the experiments of [1] such a mechanism was ruled out by the observed temperature dependence of τ_φ ($\sim 1/T$ at temperatures about

10 K). To the best of our knowledge, the behavior has not obtained a relevant explanation until now.

Recently the question seems to arise again in relation to the problem of apparent low temperature saturation of the weak localization dephasing rate which has been extensively discussed during last years, for a review e. g. Ref. [3] Namely, the correlation [3, 4] between the "saturated" dephasing rate, τ_φ^{-1}, and the diffusion constant D was reported.

This report aims to show that the correlation mentioned above can be explained within a framework of the model of tunneling states (TS) proposed in Ref [5] and considered in detail in Ref. [6]. According to this model, the dephasing is produced by dynamical structural defects with two (or more) configurations with very close energies. Due to interaction with a thermal bath these defects switch between the above states producing time-dependent fields acting upon the electrons.

There exist two mechanisms of electron dephasing due to dynamic defects. The first one is induced by direct inelastic transitions between the levels of the TS leading to a possibility of determining the actual path of the electron, and consequently to loss of interference. The second one is due to relaxation dynamics of dynamic of TSs, which fluctuate due to interaction with the thermal bath. Time dependence of the electron scattering crossection due to the defects fluctuations leads to violation of the time-reversal symmetry and, as a consequence, to decoherence. The effective Hamiltonian of a TS,

$$\tilde{\mathscr{H}}_{\mathrm{d}} = (\Delta\,\sigma_3 - \Lambda\,\sigma_1)/2\,, \tag{1}$$

is characterized by the asymmetry, Δ, and the tunneling matrix element, Λ. Since these parameters are random, their distribution, $\mathscr{P}(\Delta, \Lambda)$, is crucially important. In crystalline materials, it is naturally to assume that the TSs keep intrinsic crystal symmetry. As a result, the Λ-distribution is limited from above by some value Λ_0. To keep the model simple it is sufficient to assume that $\mathscr{P}(\Delta, \Lambda) \propto \delta(\Lambda - \Lambda_0)$.

To evaluate the distribution over Δ let us assume [5] that the distribution is due to some mesoscopic disorder around a generically symmetric defect and consider adiabatic renormalization of the site energy ε_1 of one of TS component due to conduction electrons scattered by some defect i, [5]

$$\varepsilon_{1i} = V_1 \Re\left[\sum_{\mathbf{k}} \frac{f_i(\theta)}{R_{1i}} \frac{e^{ikR_{1i}(1-\cos\theta)}}{1 + e^{(\varepsilon_{\mathbf{k}} - \varepsilon_F)/k_B T}}\right] .$$

Here $\theta = \angle\{\mathbf{k}, \mathbf{R}_{1i}\}$, f_i is the scattering amplitude by the ith defect, $\mathbf{R}_{1j}$ is the vector connecting the sites 1 and i, while V_1 is the potential of the defect 1. This

correction is due to Friedel oscillations of the electron density induced by the defect i. Assuming that the scattering potentials for the defects 1 and i are the same we get an order-of-magnitude estimate for this quantity as

$$\varepsilon_{1i} \approx -\frac{|V|^2}{\varepsilon_F} \frac{\cos(2k_F R_{1i})}{(k_F R_{1i})^3} .$$

Now let us consider a TS formed by the site 1 and some state 2, such as $R_{12} \ll R_{1i}, R_{2i}$. Then the effective two-level system acquires the diagonal splitting $\Delta_i \equiv (\varepsilon_{1i} - \varepsilon_2)$ given by the expression

$$\Delta(\mathbf{R}_i, \mu) \approx \frac{2|V|^2}{\varepsilon_F} \frac{\sin(k_F R_{12}\mu) \cdot \sin(2k_F R_i)}{(k_F R_i)^3} . \tag{2}$$

Here $\mathbf{R}_i = \mathbf{R}_{1i} \approx \mathbf{R}_{2i}$, $\mu = \cos\angle\{\mathbf{R}_{12}, \mathbf{R}_i\}$. The probability to find a TS with the splitting Δ is then

$$W(\Delta) = 2\pi n_d \int R^2\, dR \int_{-1}^{1} d\mu\, \delta\left[\Delta - \Delta(\mathbf{R}, \mu)\right] . \tag{3}$$

Here n_d is the density of defects, while $\Delta(\mathbf{R}, \mu)$ is given by Eq. (2). The density of TSs is given as $\mathscr{P}(\Delta) = N_{TS} W(\Delta)$ where N_{TS} is the density of TSs. Note that the integral in Eq. (3) is determined by $R \lesssim N_D^{-1/3}$ since the contributions of different defects have quasi-random signs, the main contribution being due to the nearest defect.

A straightforward analysis shows that there is a characteristic energy

$$E^* = \frac{|V|^2 n_d}{\varepsilon_F k_F^3} \approx \frac{1}{2\pi} \frac{\hbar}{\tau_{el}} \sim \frac{\hbar v_F^2}{D} \tag{4}$$

where τ_{el} is the elastic mean free time. At $\Delta \gg E^*$ the probability $W(\Delta)$ decays $\propto E^*/\Delta^2$, while at $\Delta \lesssim E^*$ the function $W(\Delta)$ is smooth. As a result, we arrive to the model for the density of TSs adopted in Ref. [6],

$$\mathscr{P}(\Delta, \Lambda) \approx (N_{TS}/E^*)\, \delta(\Lambda - \Lambda_0) . \tag{5}$$

As shown in Ref. [6], the two of the contributions to the dephasing rate τ_φ^{-1} can be estimated in the relevant temperature region as

$$\tau_{\varphi,in}^{-1} \sim \tau_\Lambda^{-1} = \nu_{TS}(\Lambda_0/E^*) \tag{6}$$

for "inelastic" channel and

$$\tau_{\varphi,e}^{-1} \sim \tau_{\Lambda}^{-1}(T\tau_{\Lambda}/\hbar)^{1/3} \tag{7}$$

Thus the resulting rate can be written as an interpolation

$$\tau_{\varphi}^{-1} = \tau_{\Lambda}^{-1}\left[\alpha(T\tau_{\Lambda}/\hbar)^{1/3} + \zeta\right]. \tag{8}$$

Here ν_{TS} is the effective collision frequency with the tunneling defects, α and ζ are constants of the order 1. Since $\tau_{\Lambda}^{-1} \propto D$ we conclude that for a fixed number of tunneling defects the "saturated" dephasing rate *increases* with the diffusion constant D, the corresponding dependence of τ_{φ}^{-1} tends to direct proportionality when the two items in Eq. (8) are comparable.

To make estimated we rewrite the expression for ν_{TS} in the form

$$\nu_{TS} = \sigma_e^{\mathrm{d}} v_F n_d \tag{9}$$

where σ_e^{d} is the cross-section of elastic electron scattering by a dynamic defect. Correspondingly, the key parameter of our theory, τ_{Λ}, is given as

$$\tau_{\Lambda}^{-1} = \Lambda_0 P_d \sigma_{\mathrm{in}} v_F \tag{10}$$

where $P_d = n_d/E^*$ is the density of states of the dynamic defects.

The density of states P_d can be, in principle, estimated for a given material on the base of point contact measurements. Namely, metallic point contacts are known to exhibit, first, telegraph resistance noise[7] and, second, zero-bias anomalies [8]; both effects are expected to be associated with the dynamic defects [7, 8, 5].

Although we appreciate that the material preparation procedure can significantly affect the defect system, we believe that such experiments can provide more or less reasonable estimates for P_d. The telegraph noise studies [7] for Cu nanoconstriction with a size of $\sim$ 10 nm revealed a presence of about several dynamic defects at energies less than 10 mV. This would give us the value $P_d \sim (3{-}5) \times 10^{32}$ erg^{-1}cm^{-1}. However, the telegraph noise is related to TLS with rather slow relaxation rates ($\lesssim 10^3$ s^{-1}) while we are interested in the defects with switching times of the order of 10^{-9} s. Consequently, these estimates most probably significantly *underestimate* P_d. What is more instructive, the magnitude of the resistance noise revealed rather large defect asymmetry corresponding to the estimate $\sigma_{\mathrm{in}} \sim \sigma_e^{\mathrm{d}} \sim 10^{-15}$ cm^2.

We believe that the zero bias anomalies can give more reliable information concerning P_d. The magnitude of these anomalies for Cu nanoconstrictions[8]

of the same type as mentioned above corresponds to a presence of several tens of TLS at the energy region about 1 meV [8, 5]. Correspondingly, one obtains $P_d \sim (3-5) \times 10^{34}$ erg^{-1}cm^{-3}.

Basing on these estimates and taking $P_d \approx 10^{34}$ erg^{-1}cm^{-3}, $\sigma_{\text{in}} \approx 10^{-15}$ cm^2, $v_F \approx 10^8$ cm/s, and $\Lambda_0 \approx 10$ mK we obtain $\tau_\Lambda \approx 10^{-9}$ s. Equations (9) and (10) yield $T_\Lambda \simeq \Lambda_0$. Thus at temperatures larger than $T_\Lambda \approx \Lambda_0 \approx 10$ mK one expects, according to Eq. (8), temperature-independent contribution of resonant processes.

For the relaxation channel, one obtains $T_\alpha \approx T_\beta \approx 10$ mK. Consequently, at $T \gtrsim T_\alpha \approx T_\Lambda \approx 10$ mK one expects that dephasing rate obeys Eq. (8) with $\tau_\Lambda \approx 10^{-9}$ s.

Now let us check if our assumption $\Lambda_0 \approx 10$ mK realistic. We will exploit a crude estimate

$$\Lambda_0 \simeq \frac{\hbar\omega_0}{\pi} \exp\left(-\frac{2}{\hbar}\int_0^a dr\,\sqrt{2MU(r)}\right) \tag{11}$$

where $U(r)$ is a potential relief between the two stable defect positions separated by a distance a, and M is the defect mass. Taking as an example $U(r) = (U_0/2)\,[1-\cos(2\pi r/a)]$ one obtains for the exponent $(2a/\pi\hbar)\sqrt{2U_0M}$. Taking for a light defect $\omega_0 \approx 10^{14}$ s^{-1} and assuming $a \approx 10^{-8}$ cm, $U_0 \approx 0.2$ eV one estimates that the value $\Lambda = 10$ mK is achievable for $M \approx 2 \times 10^{-23}$ g which corresponds to atomic weight ≈ 10.

Summarizing our estimates, we can conclude that for realistic parameters of the dynamic defects one can indeed expect a slow temperature dependence of the dephasing rate given by Eq. (8) crossing over to a rapid decrease at low temperatures. The crossover temperature, as well as the behavior below than that temperature, depends on the distribution of Λ. For a delta-like distribution of Λ the TLS spectrum has a gap of Λ_0. Thus the TLS contribution to dephasing rate is exponentially frozen out at for $T < \Lambda_0$, and we are left with the "standard" mechanisms like electron-electron scattering. However for the Gaussian distribution of Λ with the variance $\bar{\lambda} \gg 1$ the situation is different. In this case the cut-off temperature is given by the renormalized tunneling coupling, $\Lambda_0 e^{\bar{\lambda}}$ while for lower temperatures one deals with rather flat distribution of λ within the region $\lambda \leq \lambda_0 + \bar{\lambda}$. Correspondingly, at these temperatures one deals with a glass-like TLS distribution for which $\tau_\varphi \propto T^{-1}$.

One notes that the correlation between the dephasing rate and diffusion coefficient does not depend on the fact of "saturation" of dephasing. It depends only on the two assumptions: (1) the density of dynamic defects is given, (2) the density of states is proportional to $1/E^*$ where the scatter of the defect energies E^* is controlled by the disorder. Consequently, if the two factors mentioned above are at the stage, the correlation between τ_φ^{-1} and the diffusion constant D should

exist not only in the region of "saturated" dephasing. Here we return to the results obtained for three-dimensional low-resistivity In_2O_{3-x} films [1] where the observed temperature behavior of τ_φ corresponded to $\tau_\varphi^{-1} \propto T$. We would like to note that the systems in question, first, exhibited rather strong disorder (the elastic mean free times as small as $(2-5)\cdot 10^{-15}$ s), second, some particular disorder was expected to be related to oxygen non-stoheometry distribution. These systems are expected to be some different from the ones where the saturation of dephasing was typically studied (see e.g. [3, 4]) and which we mostly had in mind in our paper [6]. First, in the case of In_2O_{3-x} there is a probable candidate to the role of the mobile defects — oxygen atoms, the number of relevant ones is expected to be fixed for a given x. Then, the large degree of disorder makes it possible to expect that the barriers for the "mobile" defects are also affected. In particular, the expected magnitude of the Friedel oscillations is also expected to be much larger than for typical metallic crystals and their effect on the barriers can be significant. As a result, the potential for the "mobile" atoms can be equivalent to the "glassy" one allowing in particular "soft" configurations with weak barriers. If so, the relaxation rates for the TLS are expected to have a temperature behavior typical for glasses — $\tau^{-1} \propto T$ — although at the same time the density of states is still scaled with a degree of disorder. These considerations explains the experimental results by Ovadyahu [1].

To conclude, we have demonstrated that the model of tunneling states formed by light defects in crystalline conductors and affected by electronic mesoscopic disorder can explain both of the puzzles mentioned above — that is low temperature saturation-like behavior of the dephasing and the correlation between the dephasing rate and the static disorder.

Bibliography

[1] Z. Ovadyahu, Phys. Rev. Lett., **52** 569 (1984).
[2] A. Schmid Z. Phys. **271**, 251 (1974).
[3] J. J. Lin, T. J. Li, and Y. L. Zhong, cond-mat/0209275
[4] J. J. Lin and L. Y. Kao, J. Phys. C: Condens. Matter **13**, L119 (2001).
[5] V. I. Kozub and A. M. Rudin, Phys. Rev. B, **55**, 259 (1997).
[6] V. V. Afonin, J. Bergli, Y. M. Galperin, V. L. Gurevich, and V. I. Kozub, Phys. Rev. B, **66**, 165326 (2002).
[7] K. S. Ralls and R. A. Buhrman, Phys. Rev. Lett., **60**, 2434 (1988).
[8] D. C. Ralph and R. A. Buhrman, Phys. Rev. Lett., **69**, 2118 (1992).

What is hot in superconductivity: physics of vortex matter

Yu. M. Galperin[1] and V. M. Vinokur[2]

[1] Ioffe Physico-Technical Institute of RAS, 194021 St. Petersburg, Russia and University of Oslo, PO Box 1048 Blindern, 0316 Oslo, Norway

[2] Argonne National Laboratory, 9700 S. Cass av., Argonne, IL 60439, USA

1. Introduction

The aim of this lecture series is to give an introduction to the field of so-called vortex matter in superconductors. This concept is crucial for understanding the physics of type-II superconductors (materials mostly important for practical applications), as well as many micro- and nanostructured systems including superconductors. Virtually all new superconducting compounds discovered after early 60-ies up to the present time are type-II superconductors. They include organic superconductors, A-15, Chevrel phases, heavy-fermionic materials, fullerenes and high-T_c superconductors. One could say, that now type-I superconductors have become exotic. Type-II superconductivity and physics of vortex matter, as well as physics of anisotropic Fermi liquids, were the subject of Nobel Prize 2003 awarded to V. L. Ginzburg, A. A. Abrikosov, and A. J. Leggett.

The lectures are organized as follows. In the first lecture (Yu. Galperin), a historical introduction based partly on the paper [1] and partly on the press release of the Nobel Committee will be given. Basic properties of type-II superconductors will also be discussed. The second and the third lectures (V. Vinokur) will be devoted to the influence of disorder on the vortex motion. Here the concepts of pinning of the vortices, vortex glassy states, etc, will be considered.

2. Brief history

Superconductivity, one of the most interesting and unusual phenomena in solid-state physics, first became known on April 28, 1911, at the meeting of the Royal Academy of Sciences in Amsterdam, when the Dutch physicist Heike Kamerlingh Onnes reported a recently discovered effect: the complete disappearance of electrical resistance of mercury cooled by liquid helium to 4.15 K. Though no one expected this discovery, and it contradicted the existing classical electron theory of

metals, the fact that it was Kamerlingh Onnes who discovered superconductivity was not accidental. Actually, he was the first scientist who managed to solve the most complicated scientific and technical problem of the time: obtaining liquid helium (which boils at 4.16 K). This allowed scientists to peek into the unknown world of temperatures close to the absolute zero. Kamerlingh Onnes immediately tried to apply the new experimental means and to investigate the low-temperature behavior of pure metals. This was the time of hot theoretical debate whether resistance of pure metals disappears or remains finite at absolute zero. Being the advocate of the first side Kamerlingh Onnes was clearly satisfied by the result that he had obtained for mercury. But soon he realized that the vanishing of resistance at finite temperature is an effect quite different from the expected one.

It is worth emphasizing that the resistance of a sample in the superconducting state is equal to zero not approximately but *exactly*. That's why electric current in a closed circuit can circulate as long as you like without damping. The maximal duration of a non-damped superconducting current recorded in England was about two years. (The current in the ring would have circulated up till now but for a strike of transport workers which caused a break in the supply of liquid helium to the laboratory.) Even after the two years, no damping of the current was detected. Very soon superconductivity was discovered not only in mercury but in other metals as well. The prospects for practical applications of the discovered phenomenon seemed unlimited: power transmission lines without waste, powerful magnets, electric motors, new types of transformers, etc. But there were two obstacles.

The first were the extremely low temperatures at which superconductivity was observed in all materials known by the time. To cool conductors to these temperatures, the scarce helium is used (its stocks are limited, and even now producing a liter of liquid helium costs some dollars). This makes many projects to apply superconductivity simply unprofitable.

The second obstacle discovered by Kamerlingh Onnes was that superconductivity had turned out to be rather sensitive to magnetic fields and to the value of current. In fact, it was destroyed by strong fields.

The next fundamental property of the superconducting state discovered in 1933 was the Meißner–Ochsenfeld effect: the complete expulsion of magnetic field from the volume of superconductor. But again experimental investigations were complicated by the need to work with scarce liquid helium — before the World War II it was produced in about 10 laboratories throughout the world (the two of those were in the Soviet Union).

The fundamentals of superconductivity stayed absolutely out of reach of classical theory of metals whereas the quantum one was in embryo yet. The so-called

two-liquid model suggested a coexistence of two types of electrons in superconducting metals: the normal electrons interact with lattice but superconducting ones for some reason don't. This assumption let brothers London to write down the equations of electrodynamics of superconductors that described the Meißner effect and some other features. Still the microscopic mechanism of superconductivity remained a mystery.

In 1938 P. L. Kapitsa discovered the superfluidity. It turned out that at temperatures below 2.18 K liquid helium can flow through whatever thin capillary tubes without any viscosity. The theoretical explanation of this phenomenon by L. D. Landau gave rise to hopes that the theory of superconductivity was in the offing. It turns out that helium atoms at low temperature behave like quantum particles with whole spin and get accumulated at the lowest energy level (the Bose-condensation). Landau has shown that a gap that appears as the result in the spectrum of excitations makes possible the existence of the superfluid state. Discussing this macroscopic revelation of the entirely quantum effect Landau called helium "a window to the quantum world".

A straightforward extension of these ideas to superconductivity failed. The reason was that electrons are particles with spin one-half (so-called fermions) and behave absolutely unlike helium atoms which possess a whole spin being bosons. In quantum system of electrons excitations with zero energy may appear even at zero temperature and the Landau criterion of superfluidity does not hold.

The natural desire to reduce the problem to that already solved inspired the idea to prepare of two fermions a composite boson with a whole total spin and after that to effect the Landau superfluidity scenario. However this was opposed by Coulomb repulsion of electrons that was too strong in spite of screening that occurs in electro-neutral metal.

A little later Frölich and Bardeen have independently demonstrated that interaction of electrons with lattice oscillations (phonons) may lead to attraction. This could in principle overcome the electrostatic repulsion but one had to keep in mind the huge kinetic energies of electrons. At the first sight those should break the just found weak coupling. Composite bosons did not work out.

In the same 1950 with the help of experimental data and theoretical achievements of solid-state physics, based on quantum mechanics and statistical physics, V. L. Ginzburg and L. D. Landau (USSR) developed a phenomenological theory of superconductivity, known as the Ginzburg–Landau (GL) theory. It proved so successful and predictive that even now it remains a powerful research tool despite that the 50 elapsed years were marked by the creation of the microscopic theory of superconductivity. We will discuss the GL theory in more detail in Sec. 4.

In 1957 the American scientists John Bardeen, Leon Cooper and Robert Schri-

effer put together the mentioned above ideas and hints and created a consistent microscopic theory of superconductivity. It was found that superconductivity is indeed linked with the appearance of a peculiar attraction of electrons in metals. This is an utterly quantum phenomenon.

We have already mentioned that the ground state of fermionic system is characterized by big kinetic energies of electrons. Luckily those do not prevent binding of low-energy excitations of the system that behave like *quasiparticles*. They have the same electric charge e as the electron and some effective mass but their energy may be whatever small. The attraction brings on a rearrangement of quasiparticle spectrum and the long-awaited gap that was so crucial for the Landau superfluidity criterion opens at last.

The origin of the attraction may be understood with the help of a far analogy with two balls lying on a rubber rug. If the balls are far from each other, each of them deforms the rug, making a little depression. But if we put a ball on the rug and place another one near the first, their holes will join, the balls will roll down to the bottom of the combined valley and lie together. In metals the mechanism is realized by deformations of crystal lattice. At low temperatures some quasiparticles (usually they are called, just the same, electrons) form a sort of bound pairs. These are called the "Cooper pairs" after the man who discovered the binding. The size of the pairs on the atomic scale is really quite large, reaching hundreds and thousands of interatomic distances. According to the graphic comparison suggested by Schrieffer, they should be envisaged not as a double star composed of electrons but rather like a couple of friends in a discotheque who either come together or dance in different corners of the hall, separated by dozens of other dancers.

It took almost half a century since the discovery to gain cardinal progress in understanding the nature of superconductivity and to develop the consistent theory. This period may be considered to be the first stage of superconductivity studies.

3. Superconductivity and magnetism

Superconductivity is characterized by electron pairs (or holes) that have condensed into a ground state, where they all move coherently. This means not only that the resistance disappears but also that a magnetic field is expelled from the superconductor (the charged superfluid). This is known as the Meißner effect. Many superconductors show a complete Meißner effect, which means that a transition from the superconducting to the normal state occurs discontinuously at a certain critical external magnetic field H_c. Other superconductors, in particular alloys, only show a partial Meissner effect or none at all. Work done in Kharkov by

L. Shubnikov and by others elsewhere showed that the magnetization may change continuously as the external field is increased, starting at a lower critical field, H_{c1}, while the superconductor continues to show no resistance up to a much higher upper critical field, H_{c2}. This effect is illustrated in Fig. 1. Between the lower and

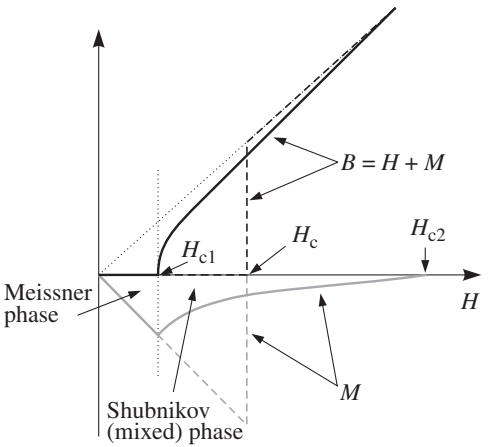

Figure 1. Magnetization M and induced field B as a function of external magnetic field H for superconductors with complete (dashed lines) and partial (full lines) Meißner effect (see text).

the upper critical fields the superconducting state coexists with a magnetic field.

The theoretical framework for understanding the behavior of superconductors in the presence of such strong magnetic fields was developed in the 1950s by a group of Soviet physicists. In a groundbreaking paper [2], published in 1957, Abrikosov discovered the vortices in the order parameter of a superconductor and described their crucial role for the coexistence of a magnetic field and superconductivity in superconductors "of the second group", or in "type-II superconductors" as we would say today. In the same paper, Abrikosov provided an amazingly detailed prediction — later to be borne out by experiments — of the way in which a stronger magnetic field suppresses superconductivity: vortices, which form a lattice, come closer to each other, and at some field the vortex cores overlap, suppressing the order parameter everywhere in the superconducting material — hence driving it into the normal state.

Abrikosov's results came from an insightful analysis of the Ginzburg–Landau equations [3], a phenomenological description of superconductivity published in 1950 by Vitaly Ginzburg and Lev Landau. One of the motivations behind their work was the need to develop a theory that would make it possible to describe

correctly the destruction of superconductivity by a magnetic field or an electric current. The Ginzburg–Landau equations have proved to be of great importance in physics, not only for describing superconductivity in the presence of a magnetic field. In their 1950 paper Ginzburg and Landau were the first to realize that superconductors can be divided into two classes with regard to their behavior in a magnetic field. They introduced a quantity $\varkappa$, now known as the Ginzburg–Landau parameter, which enabled them to make a distinction between the two classes. Superconductors with $\varkappa < 1/\sqrt{2}$ do not allow the coexistence of a magnetic field and superconductivity in the same volume. Superconducting materials with $\varkappa > 1/\sqrt{2}$ do allow for such a coexistence. In modern language $\varkappa = \lambda/\xi$ is the ratio of the magnetic field penetration length λ and the coherence length ξ.

The superconductors known at the time had $\varkappa \ll 1$, e.g., for Hg $\varkappa \approx 0.16$, beyond showing that if a material with $\varkappa \geq 1/\sqrt{2}$ is placed in a magnetic field somewhat larger than the thermodynamic critical value, the normal phase is unstable with respect to formation of a superconducting state. However, they introduced the crucial notions of a superconducting order parameter, of negative surface energy of the boundary separating the superconducting from the normal phase in type-II superconductors, and (in modern terminology) of the upper critical magnetic field, where superconductivity vanishes in type-II materials. Even so, it was left to Abrikosov to describe in 1952 the result of this instability and to formulate the complete phenomenological theory of type-II superconductors. At the same time it is clear that the Ginzburg–Landau equation and the partial understanding achieved by Ginzburg and Landau was a necessary basis for his work.

4. Ginzburg–Landau theory

The GL theory [3] is based on Landau's theory of second order phase transitions from 1937. This was a natural starting point, since in the absence of a magnetic field the transition into the superconducting state at a critical temperature T_c is a second-order phase transition. Landau's theory describes the transition from a disordered to an ordered state in terms of an "order parameter", which is zero in the disordered phase and nonzero in the ordered phase. In the theory of ferromagnetism, for example, the order parameter is the spontaneous magnetization. In order to describe the transition to a superconducting state, GL took the order parameter to be a certain complex function $\Psi(\boldsymbol{r})$ which they interpreted as the "effective" wave function of the "superconducting electrons", whose density n_s is given by $|\Psi(\boldsymbol{r})|^2$; today we would say that $\Psi(\boldsymbol{r})$ is the macroscopic wave function of the superconducting condensate.

In accordance with Landau's general theory of second-order phase transitions,

the free energy of the superconductor depends only on $|\Psi(\boldsymbol{r})|^2$ and may be expanded in a power series close to T_c. Assuming first that $\Psi(\boldsymbol{r})$ does not vary in space, the free energy density becomes

$$f_s = f_n + \alpha|\Psi|^2 + \beta|\Psi|^4 + \dots \tag{1}$$

where the subscripts n and s refer to the contributions from the normal and the superconducting state respectively. A stable superconducting state is obtained if β is a positive constant and $\alpha = \alpha_0(T - T_c)$.

Since the purpose of Ginzburg and Landau was to describe the superconductor in the presence of a magnetic field, H, when the order parameter may vary in space, gradient terms had to be added to the expansion. The lowest order gradient term looks like a kinetic energy term in quantum mechanics, which is why GL wrote it — adding a term for the magnetic field energy — as

$$\frac{1}{2m^*}\left|\left(-i\hbar\boldsymbol{\nabla} - \frac{e^*}{c}\boldsymbol{A}\right)\right|^2 + \frac{1}{2\mu_0}(\operatorname{curl}\boldsymbol{A})^2\,. \tag{2}$$

Here the magnetic field $\boldsymbol{H} = \mu_0^{-1}\operatorname{curl}\boldsymbol{A}$ is described by its vector potential, $\boldsymbol{A}(\boldsymbol{r})$, which enters the kinetic energy term as required by gauge-invariance. The total free energy F_s is obtained by integrating the free energy density f_s over volume.

By minimizing the free energy Fs with respect to Ψ, Ψ^* and $\boldsymbol{A}$, the GL equations are obtained. They are

$$\frac{1}{2m^*}\left(-i\hbar\boldsymbol{\nabla} - \frac{e^*}{c}\boldsymbol{A}\right)^2\Psi + \alpha\Psi + \beta|\Psi|^2\Psi = 0\,, \tag{3}$$

$$\boldsymbol{j} = \operatorname{curl}\boldsymbol{H} = \frac{e^*\hbar}{2m^*c}(\Psi^*\boldsymbol{\nabla}\Psi - \Psi\boldsymbol{\nabla}\Psi^*) + \frac{e^{*2}}{m^*c^2}|\Psi|^2\boldsymbol{A} \tag{4}$$

plus a boundary condition.

The second equation has the same form as the usual expression for the current density in quantum mechanics, while the first — except for a term nonlinear in Ψ, which acts like a repulsive potential — resembles the Schrödinger equation for a particle of mass m^*, charge e^* with energy eigenvalue $-\alpha$. In their paper Ginzburg and Landau wrote that "e^* is the charge, which there is no reason to consider as different from the electronic charge". As soon as they learned about the BCS theory and Cooper pairs, however, they realized that $e^* = 2e$ and $m^* = 2m$.

The GL equations are capable of describing many phenomena. An analysis shows, for example, that a magnetic field penetrating into a superconductor

decays with its distance from the border to a normal phase region over a characteristic length $\lambda(T)$ where $\lambda^2(T) = \beta m^*/|\alpha|e^{*2}$. This is the London penetration length. Furthermore, it is found that a disturbance $\delta\Psi$ from an equilibrium value of the order parameter, decays over a characteristic length ξ, where $\xi^2 = \hbar^2/4m^*|\alpha|$. Therefore, the penetration length λ and the coherence length ξ are two characteristic lengths in the GL theory. (Although the physics was clear to them, Ginzburg and Landau used neither this notation nor this terminology; the concept of a *coherence length* was only introduced three years later by B. Pippard). The two lengths have the same temperature dependence close to T_c, where $\lambda, \xi \propto (T_c - T)^{-1}$.

At this point a short digression about the surface energy between superconducting and normal phases of the same material is called for. It follows from the GL equations that this quantity depends on the two characteristic lengths λ and ξ in a way that can be understood from Fig. 2.

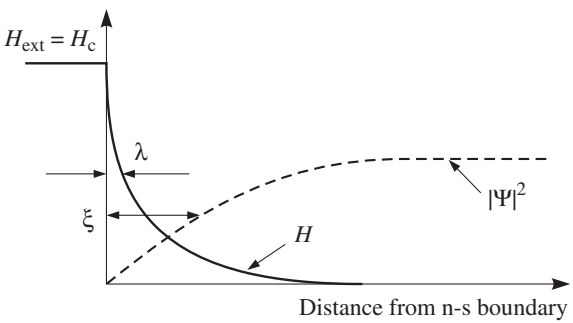

Figure 2. Sketch of the border region between a normal and a superconducting phase, illustrating the concepts of penetration length λ and coherence length ξ. If the magnetic field is H_c in the normal phase, it decays to zero in the superconducting phase over a length λ. At the same time the superconducting order increases from zero at the interface to its full value inside the superconducting phase over a distance ξ.

5. Theory of type-II superconductors

One of the physicists who soon began to test the predictions of the GL theory was the young N. V. Zavaritzkii. Working at the Kapitsa Institute for Physical Problems in Moscow, he was able to verify the theoretical predictions about the dependence on film thickness and temperature of the critical magnetic field of superconducting films. However, when he tried to make better samples by a new technique (vapor deposition on glass substrates at low temperatures) he discovered that the critical fields no longer agreed with the GL theory. He brought this to the attention of his

room mate at the university, Alexei Abrikosov. Abrikosov looked for a solution to this mystery within the GL theory and started to think about the true nature of the superconducting state for $\varkappa \equiv \lambda/\xi > 1/\sqrt{2}$. In contrast to the superconductors that were the focus of Ginzburg's and Landau's interest in 1950, the new materials had values in this parameter regime. In 1952 Abrikosov [2] was able to calculate the critical magnetic fields for this parameter regime and found agreement with Zavaritzkii's measurements.

Abrikosov continued to think about strongly "type-II superconductors" with large values of $\varkappa$. It was clear that superconductivity could not exist in magnetic fields of a certain strength. But Abrikosov was able to show that when the field is diminished again, small superconducting regions start to nucleate at a magnetic field $H_{c2} = H_c\varkappa\sqrt{2}$, which for $\varkappa > \sqrt{2}$ is larger than the thermodynamic critical field H_c. The latter is the critical field that is relevant for normal, or "type-I" superconductors. We now call H_{c2} the *upper* critical magnetic field. However, the material is not completely superconducting in the sense that the magnetic field vanishes everywhere in the material. Abrikosov found that a periodic distribution of the magnetic field, as a lattice, minimized the total energy. The flux of the magnetic field through an elementary cell of the vortex lattice is a universal constant, $\Phi_0 = \pi\hbar c/2e \approx 2.05 \cdot 10^{-7}$ G$\cdot$ cm^2. An experimentally observed Abrikosov lattice of this type is shown in Fig. 3.

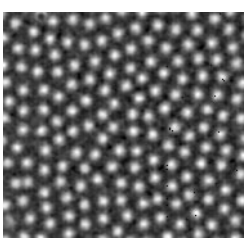

Figure 3. Abrikosov lattice of magnetic flux lines (vortices) in $NbSe_2$ — a type-II superconductor — visualized by magneto-optical imaging at the Oslo University. This picture was used for the Nobel Prize 2000 press release. The first pictures of such a vortex lattice were taken in 1967 by U. Essmann and H. Träuble, who sprinkled their sample surfaces with a ferromagnetic powder that arranges itself in a pattern reflecting the magnetic flux line structure.

The approach that worked for magnetic fields just below the upper critical field, where the order parameter is small and the nonlinear term in the first GL equation can be neglected, does not work for much weaker fields. However, by studying the nature of the solutions for fields just below H_{c2}, Abrikosov realized that they correspond to vortices in the order parameter and that this type of solution must

be valid for weaker fields as well.

The point is that because we require the theory to be gauge invariant, the vector potential $\boldsymbol{A}$ and the phase φ of the order parameter $\Psi = |\Psi|e^{i\varphi}$ appear in the combination $\boldsymbol{A} - (\hbar c/2e)\boldsymbol{\nabla}\varphi$ in the first GL equation. Now, for the magnetic field to be constant inside the superconductor A has to grow. If the free energy is not to grow without limit, the growth in the vector potential has to be compensated by jumps in the phase. It turns out that this corresponds to vortex solutions in which the order parameter vanishes at the points of a regular (triangular or hexagonal) lattice and the phase of the order parameter changes by 2π on a closed contour around these lattice points.

Abrikosov discovered these solutions in 1953, but they were unexpected and he did not publish them until 1957. The suggestion by R. P. Feynman in 1955 that vortex filaments are formed in superfluid ^{4}He had then reached the Soviet Union. The level of scientific contact between East and West was very low during the Cold War and the work of Soviet scientists did not, in general, get much attention from researchers in the West. The work of Ginzburg–Landau was received with scepticism until L. P. Gorkov showed in 1959 that the GL equations could be derived from the microscopic BCS theory in the appropriate limit. The work of Abrikosov was not fully appreciated in the West until the 1960s, when superconductors with very high critical fields had been discovered.

6. Importance

The Ginzburg–Landau (GL) theory has been important in many fields of physics, including particle physics, where it is used in string theory. Today, the GL theory is extensively used to describe superconductive properties that are important in practical applications. This theory is able to describe, for example, spatially varying superconducting order, superconductivity in strong magnetic fields.

Abrikosov's theory of superconductors in a magnetic field created a new field of physics — the study of type-II superconductors. After the discovery in 1986 of the ceramic "high-temperature" superconductors, which are extreme type-II superconductors, by Gerd Bednorz and Alex Müller (Nobel Prize 1987) research to understand and use these new materials has become a very large activity. The vortex/flux lines discovered by Abrikosov are very important for the properties of these materials — the term "vortex matter" is used.

7. Vortex line as an elastic object

Abrikosov vortices in type II superconductors appear as the special nontrivial solution of Ginzburg–Landau energy functional. However in the case of strongly

type II materials, $\lambda \gg \xi$, for almost all the practical purposes vortex matter is very well described within the *London theory*, which neglects spatial variations of the modulus of the order parameter $|\Psi|$. In the London theory the total system energy is represented as energy of the currents flowing in the superconductor and energy of the magnetic field $B^2/8\pi$. Positions of vortices are defined as points of singularities of the phase of the order parameter. Considering the case of only one vortex line, one can integrate the energy in the plane perpendicular to the vortex, one can calculate the energy per unit vortex length as $e_{\rm el} = \varepsilon_\circ \ln(\lambda/\xi)$, where $\varepsilon_\circ = \Phi_\circ/(4\pi\lambda)^2$. Thus within the London approximation vortex can be viewed as the elastic line with the linear tension $\varepsilon_l = e_{\rm el}$. Finally, the energy of the system of the vortex lines assumes the form:

$$\mathscr{F} = \sum_i \int \mathrm{d}z \frac{\varepsilon_l}{2} \left(\frac{\partial \mathbf{u}_i}{\partial z} \right)^2 + \sum_{i,j} \int \mathrm{d}z \, \mathrm{d}z' v[\mathbf{u}_i(z) - \mathbf{u}_j(z')], \tag{5}$$

where $\mathbf{u}_i(z)$ is the lateral displacement of the i-th vortex. The second term represents interactions between the vortex lines. In the most cases however one can consider only the "equal z" interactions.

8. Collective pinning

The concept of weak collective pinning [4] is illustrated by a single vortex line subject to weak disorder [5]. Point defects acting on the elastic line compete with each other. When summing up pinning forces, the individual pins add up statistically, giving zero on average. Thus vortex line gets pinned only by the fluctuations in defect density, and the total force exerted on the segment L is $\mathscr{F}_{\rm pin} \simeq (f_{\rm pin}^2 n_i \xi^2 L)^{1/2}$, where $f_{\rm pin}$ is the individual pinning force and the coherence lengthξ lays the role of the spatial scale of the pinning potential; n_i is the point defect density (See Fig. 4).

In the presence of the applied current pinning force has to compete with the Lorentz force, $\mathscr{F}_{\rm L} \simeq j\Phi_0 L/c$. Since $\mathscr{F}_{\rm L} \sim L$, while $\mathscr{F}_{\rm pin} \sim \sqrt{L}$, Lorentz force always wins at large distances. This means that stiff vortex cannot be pinned. Pinning is achieved by adjusting flexible vortex to pinning relief; the adjustment scale $L_{\rm c}$ is determined by the balance $\mathscr{E}_{\rm el}(L_{\rm c}) \simeq \varepsilon_\circ \xi^2/L_{\rm c} \sim \mathscr{E}_{\rm pin}(L_{\rm c})$. At $L > L_{\rm c}$, the vortex splits into the effectively independently pinned segments. Thus the total pinning force on the length L appears to be proportional to the number $L/L_{\rm c}$ of the Larkin segments on the length L, i.e. total pinning force now $\propto L$. The critical current $j_{\rm c}$, i.e. the current until which vortices remain immobile is given by the condition $\mathscr{F}_{\rm pin}(L_{\rm c}) = \mathscr{F}_{\rm L}(L_{\rm c})$ and is $j_{\rm c} = j_\circ(\xi\gamma/\varepsilon_\circ^2)^{2/3}$, $\gamma \simeq n_i \xi^2 f_{\rm pin}^2$, $j_\circ$ is the pairbreaking current. On a more formal level, point defect pinning is described by

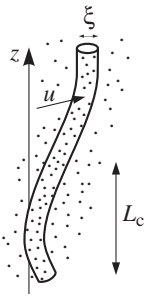

Figure 4. Single vortex line pinned by the collective action of many weak pointlike pinning centers. Only fluctuations in the pin density are able to pine the vortex. In order to accommodate optimally to the pinning potential, the vortex line deforms by ξ (the minimal transverse scale for the vortex core is able to resolve equals to the scale of the pinning potential) on a longitudinal scale L_c, the collective pinning length.

addition to the free energy density of Eq. (5) the term $\varepsilon_{\rm pin}(\mathbf{u}_i, z)$ with the statistical properties $\langle \varepsilon_{\rm pin}(\mathbf{u}_i, z)\varepsilon_{\rm pin}(\mathbf{0}, 0)\rangle = \gamma\delta(\mathbf{u})\delta(z)$.

At finite temperatures vortices fluctuate near their equilibrium positions and smoothen pinning potential [6]. The effect of these phonon-like oscillations is very similar to the suppression of Bragg peaks in the usual lattice due to oscillations of atoms: peak intensity is reduced by the Debye–Waller factor. Analogously, pinning potential effectively weakens and critical current decreases exponentially above some characteristic depinning temperature $T_{\rm depin} \simeq (\gamma\varepsilon_\circ\xi^2)^{1/3}$. Below we show how the temperature dependence of the critical current can be obtained from the quantum mechanical mapping.

9. Creep

As it was mentioned above, if at zero temperature the applied current j is smaller than the critical current, $j < j_c$, vortices remain pinned. At finite temperatures however vortices can move due to processes of thermal activation. In the rugged energy landscape vortices assume positions in the local minima (valleys) of the potential relief. In the presence of the external force (bias) vortices move via a sequence of thermally activated jumps of the vortex segments between the neighboring low-lying metastable states (See Fig. 5).

The discussion of the creep dynamics starts from the fact that the geometry of the low-lying metastable states for the elastic system in the random potential is characterized by the following scaling relation for the roughness $w(L) = \langle[\mathbf{u}(\mathbf{r}+\mathbf{L})\mathbf{u}(\mathbf{r})]^2\rangle^{1/2}$, $L \gg L_c$ (on the scales $L < L_c$ vortex lines remain within the same

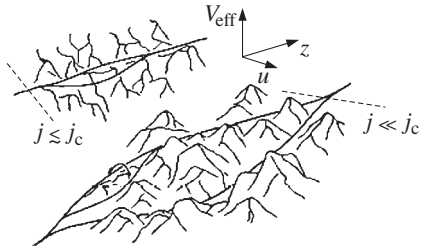

Figure 5. Effective tilted random potential felt by the flux line in the presence of quenched disorder and of a driving transport current density j. The elastic vortex line relaxes into a low-lying metastable state. Close to the critical driving force, $j \lesssim j_c$, the next metastable state is very near the original state and separated from the latter by only a small barrier $U(j) \approx U_c(1 - j/j_c)^a$. At low driving currents, $j \ll j_c$, the closest favorable metastable state is far away from the original state and separated from the latter by a large barrier $U(j) \approx U_c(1 - j/j_c)^\mu$. Hops to the closest valleys are not favorable and represent only an intermediate step in the diffusion motion of the vortex to its next optimal state.

metastable state):

$$w(L) \sim \xi \left(\frac{L}{L_c}\right)^{\zeta}, \tag{6}$$

the exponent ζ is called roughness exponent. Metastable states are determined by the competition between pinning and elastic energies. Since characteristic elastic energy is estimated as $\varepsilon_l w^2/L$, the characteristic fluctuations in the low-lying metastable states scale as $E_p(L/L_c)^\chi$, $E_p = \xi\gamma^{1/2}L_c^{D-2}$, D is the dimensionality of the space, $\chi = D - 2 + 2\zeta$. The basic assumption of the creep theory is that the random elastic system is governed by the unique energy scale [7]. This implies that the *barriers* separating low-lying metastable states also obey the same relation:

$$E_{\rm barr} \simeq E_p\left(\frac{L}{L_c}\right)^{\chi}. \tag{7}$$

In the presence of the small applied force $f = (1/c)\Phi_\circ j$, the energy for the tilted barrier can be written in a form (See Fig. 6):

$$E_{\rm barr} \simeq E_p\left(\frac{L}{L_c}\right)^{\chi} - fw(L)L^D = E_p\left(\frac{L}{L_c}\right)^{\chi}\left[1 - \left(\frac{L}{L_f}\right)^{2-\zeta}\right], \tag{8}$$

where $L_f = L_c(f_c/f)^{1/(2-\zeta)}$. The physical meaning of the length L_f is that at the scales $L < L_f$ the system is pinned and motion is possible due to thermally

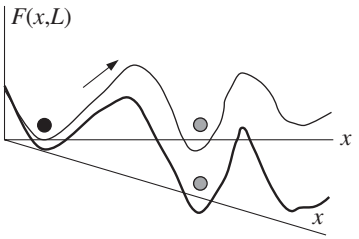

Figure 6. The changes in the coordinate energy dependence for the titled barrier.

activated processes only, while at $L > L_f$ pinning does not exist. Thus the energy barriers that control creep motion are $E_{\rm barr}(L_f) \simeq E_{\rm p}(f_{\rm c}/f)^{\mu}$, $\mu = \chi/(2-\zeta)$.

To close equations describing dynamics one can notice that relaxation processes in random systems are governed by the barriers that satisfy the basic relation

$$E_{\rm barr} \sim T \ln(t/t_0), \tag{9}$$

where t is the observation time and t_0 is some characteristic microscopic time. This relation can be understood as follows: the activation barrier E is surmounted in the time $t \sim \exp(E/T)$. This means that all the barriers with energies $E \ll E_{\rm barr}$ from (9) are long behind and thus long forgotten. On the other hand, the barriers with $E \gg E_{\rm barr}$ are unknown to the system since it did not have enough time to try to overcome them. Thus the only relevant barriers given the lifetime t are those from Eq. (9). Now combining (9) with the expression for $E_{\rm barr}(L_f)$, one arrives at the basic equation for the rate of the thermally activated vortex motion v in the presence of the small, $f < f_{\rm c}$, constant applied force [7]:

$$v \sim t^{-1} \sim \exp\left[-\frac{E_{\rm p}(T)}{T} \left(\frac{f_{\rm c}(T)}{f} \right)^{\mu} \right]. \tag{10}$$

Notice the fundamental deep character of the relation (10): the activation barrier *diverges* (as a power of the applied force f) as $f \to 0$, therefore *there is no linear response* in the system; the behavior of the system at infinitesimal forces is strongly nonlinear, even more, the velocity is the non-analytic function of the applied force.

10. Quantum mechanical mapping

In 1988 David Nelson noticed the remarkable correspondence between the statistical mechanics of the array of the vortex lines in n dimensions and quantum mechanics of Bose-particles in an $n-1$-dimensional system [8]. The mapping is

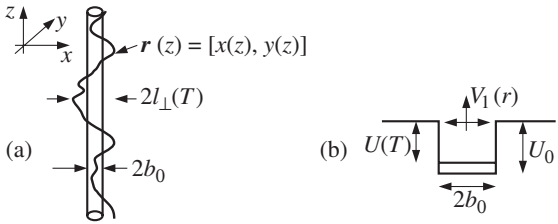

Figure 7. Schematic of a flux line interacting with a columnar pin. (a) The line is confined to a tube of radius $l_\perp(T)$. (b) Cylindrical square well potential which models the binding of the line to the pin. The binding potential is reduced from U_0 to $U(T)$ by thermal fluctuations.

realized by the vocabulary establishing correspondence between parameters of the vortex system and those for the quantum mechanical particles: $\varepsilon_l \leftrightarrow m$, $T \leftrightarrow \hbar$, system size along the magnetic field $L \leftrightarrow \hbar/T_{\rm B}$, where $T_{\rm B}$ is the physical temperature of the boson system, the electric charge of bosons $\leftrightarrow \Phi_\circ$, and the electric field that acts on charged bosons corresponds to the applied current in vortex system, $\mathscr{E} \leftrightarrow (1/c)j$. The power of this mapping can be best illustrated by consideration of pinning of vortices by the array of columnar defects that can be engineered in superconductor samples via irradiation of the latter with heavy ions (Pb, Au, U) [9]. A free energy of the vortex configuration can be written as a functional of the vortex displacements $\mathbf{r}_i(z)$ as

$$\mathscr{F} = \int_0^L \mathrm{d}z \left[\sum_i \frac{\epsilon_1}{2} \left(\frac{\partial \mathbf{r}_i}{\partial z} \right)^2 + U(\mathbf{r}_i) + \frac{1}{2} \sum_{i,j} v(\mathbf{r}_{ij}) \right] \tag{11}$$

where the interaction between the vortices is

$$v(r) = \epsilon_0 \, K_0(r/\lambda), \tag{12}$$

with K_0 being the Bessel function. The disorder potential $U(r)$ is a sum of the potential wells representing the columnar defects

$$U(r) = \sum_i u(r - r_i), \tag{13}$$

with r_i being the coordinate of the i-th defect. A columnar defect represents a strong pinning center for the vortex line due to matching between the linear geometries of the trap for the vortex line and that of the object to pin (See Fig. 7). At moderate magnetic fields where defects outnumber vortices the critical current is determined by the pinning strength of an individual columnar defect.

In the quantum mapping picture, the columnar pinning track corresponds to a trap (potential well) for a 2D particle and the critical current corresponds to the ionization of energy from this trap, i.e. to the depth of the bound state. In the case of the shallow 2D quantum well (high temperatures for vortices) of the finite radius $r_\circ$, it is given by $|E| \sim \exp[-(\hbar^2/m) \mid \int_0^\infty drrU(r) \mid^{-1}]$. Transcribing this back to vortices and estimating $\int_0^\infty drrU(r) \simeq r_\circ^2 U_\circ$ ($U_\circ$ is the strength of the columnar pinning potential), we get $j_c(T) \sim j_c(0)\exp[-(T/T^*)^2]$ with characteristic depinning temperature $T^* \simeq r_\circ\sqrt{\varepsilon_l U_\circ}$. More refined calculation that takes into account that the true pinning potential for the vortex line drops as $1/r^2$ [5, 10] with the distance r from the vortex line, gives

$$j_c(T) \sim j_c(0)\exp[-T\sqrt{2}/r_\circ\sqrt{\varepsilon_l\varepsilon_\circ}], \tag{14}$$

with $U_\circ \simeq \varepsilon_0\,(r_\circ^2/4\xi^2)$.

It is very instructive to see that this quantum mechanical mapping can be used for estimating temperature dependence of the critical current due to *point defects*. To this end we assume that vortex line pinned by point defects maps onto a 2D quantum particle trapped by some *effective* potential well. Then one can write the estimate for the ionization energy as $|E| \sim \exp(-\hbar/m\xi^2|U_{\text{eff}})$, where U_{eff} is to be determined. Turning back to a vortex line, this estimate implies

$$j_c \sim \exp(-T^2/\varepsilon_l\xi^2\tilde{U}_{\text{eff}}), \tag{15}$$

where $\tilde{U}_{\text{eff}}$ stands now for an *effective* pinning potential per unit length. In a pinned state the energy of thermal fluctuations is balanced by pinning energy; thus

$$T \sim \sqrt{\gamma L}\ , \tag{16}$$

where L is the characteristic length of the pinned segment. Then by definition $\tilde{U}_{\text{eff}} \equiv \sqrt{\gamma L}/L = \sqrt{\gamma/L} = \gamma/T$, and plugging this into the Eq. (15), we arrive at

$$j_c(T) \sim j_c(0)\exp[-(T/T_{\text{depin}})^3] \tag{17}$$

with $T_{\text{depin}} = (\varepsilon_l\gamma\,\xi^2)^{1/3}$, which is exactly the relation derived in the original paper [6] by using high vortex velocity perturbation theory with respect to disorder.

11. Creep through columnar defects

The system described by the free energy (11) represents, in a dual quantum mechanical picture, a 2D interacting Bose-system subject to strong disorder that shows a wealth of different behaviors. If disorder is sufficiently strong, Bose

particles get localized to form the so-called *Bose glass*. This corresponds to the low-temperature behavior of the related vortex system at low temperatures: the pristine vortex structure would have formed Abrikosov lattice but columnar defects cause formation of strongly pinned Bose glass [9, 11]. With the increasing temperature the Bose glass melts at the melting line $B_{\rm m}(T)$, into a vortex liquid. In the related quantum mechanical 2D Bose system the vortex liquid maps to the superfluid phase. Disorder partially destroys superfluidity: the superfluid density n_s decreases. This depletion of the superfluid density by disorder corresponds to enhancement of the average tilt modulus of the related vortex system [12, 13]. Moreover, one can expect that this stiffening is accompanied by the change in transport properties: the part of the vortices remain pinned and does not participate in transport. This may be interpreted as the intermediate vortex phase where both vortex liquid and pinned vortices coexist.

We address now the low temperature Bose glass dynamics. As we have already discussed above the main characteristic of the low temperature glassy phase is its highly nonlinear response. For brevity and illustration purposes we focus on the single vortex creep that realizes normally in the case where columnar defects significantly outnumber vortices. For the usual irradiation doses employed in experiments this corresponds to moderate fields range up to 0.1 T.

The simplest example of creep is the liberation of a single vortex from a single columnar defect (see Fig. 8). If (in the notations of Reference [9]) the half-loop

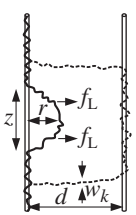

Figure 8. Half-loop and double-kink transport process for flux lines. The Lorentz force $f_{\rm L}$ attempts to push the line to the right.

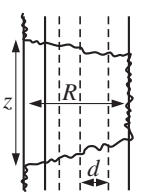

Figure 9. Double-superkink configuration required for variable-range hopping. The "tongue" of the vortex line seeks out a compatible low-energy pin so that the line can spread.

extends for a distance z along the defect, and has a lateral size r than the energy change due to formation of such a loop in the presence of the applied force $f_{\rm L} = (1/c)\, j\, \Phi_\circ$ is

$$\delta\mathscr{F} \simeq \varepsilon_l \frac{r^2}{z} + U_\circ z - f_{\rm L} r\, z \qquad (18)$$

Optimization with respect to r and z yields the saddle point values $r^* \sim U_\circ c/j\,\Phi_\circ$ and $z^* \sim c\varepsilon_l^{1/2}U_\circ^{1/2}/j\,\Phi_\circ$, and, correspondingly,

$$\delta\mathscr{F}^* \simeq \frac{c\,\varepsilon_l^{1/2}U_\circ^{3/2}}{\Phi_\circ\, j} \tag{19}$$

Identifying this energy change with the activation barrier we arrive at the conclusion that the escape rate for the vortex from a columnar defect is $v \sim \exp(-\delta\mathscr{F}^*/T)$. Each vortex moving with the velocity v generates the electric field $\mathbf{E} = (\Phi_\circ/c)[\hat{\mathbf{z}} \times \mathbf{v}]$, the voltage measured in the sample where vortex motion is governed by vortex depinning from columnar defects will be

$$V \propto \exp\left(-\frac{4\sqrt{2}c\,\varepsilon_l^{1/2}U_\circ^{3/2}}{3\Phi_\circ\, j}\right) \tag{20}$$

(numerical factor $4\sqrt{2}/3$ is obtained by the exact variational calculation of the saddle configuration for the vortex escape from the cylindrical cavity). It is most remarkable that by quantum mechanical mapping $\varepsilon_l \to m$, $T \to \hbar$, and $\Phi_\circ\, j/c \to |eE|$, one immediately recovers from (20) the well known quantum-mechanical result for the cold ionization from the 2D potential well [14].

At smaller currents the lateral size of the vortex half loop grows and the dynamic regime where vortex lines hop from one columnar defect to neighboring ones favored by the applied current (see Fig. 8). Even more interesting dynamics occurs at yet smaller currents where vortex loop can sample *many* columnar defects choosing the optimal one for the jump (Fig. 9). Using quantum-mechanical mapping and mobilizing the quantum-mechanical intuition, one can guess that the resulting mechanism of vortex motion becomes the equivalent of the 2D variable range hopping, i.e. the voltage measured in such a regime becomes:

$$V \propto \exp\left[-\frac{E_{\mathrm{VRH}}}{T}\left(\frac{J_{\mathrm{VRH}}}{J}\right)^{1/3}\right] \tag{21}$$

Experiments on high temperature superconductors indeed revealed the existence of both dynamic regimes (see Figs. 10–11) Moreover even the effects that stem from the interactions of the vortex lines and are equivalent to the *Coulomb gap* phenomenon are observed in a full analogy with the behavior of conductivity of semiconductors in two dimensions.

12. Conclusion: creep dynamics

Reviewing our above considerations and illustrative examples of creep, one can notice that basically our discussion had a very general character and that the only

Superfast Vortex Creep in $YBa_2Cu_3O_{7-\delta}$ Crystals with Columnar Defects: Evidence for Variable-Range Vortex Hopping

J. R. Thompson,[1] L. Krusin-Elbaum,[2] L. Civale,[3] G. Blatter,[4] and C. Feild[2]

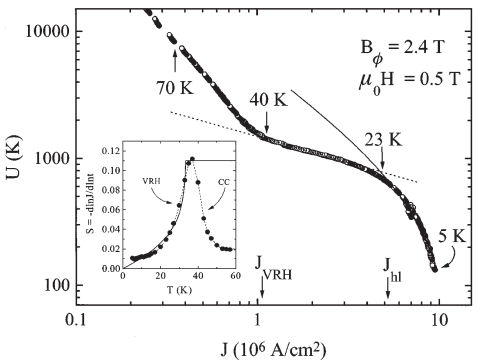

FIG. 4. $U(J)$ for the $B_\Phi = 2.4$ T crystal in a 0.5 T magnetic field. The solid line is the fit to the full glassy expression for $U(J)$ (see text) with $\mu \simeq 1$. The slope $\mu \sim 1/3$ (dashed line) fits the data well between 23 and 40 K. Crossover currents are indicated by the arrows. Inset: Fit to variable-range hopping [Eq. (3)] with $\mu = 1/3$ (see text) is shown as the solid line. The decreased rate on the high-T side of the peak is due to slower creep in the collective regime.

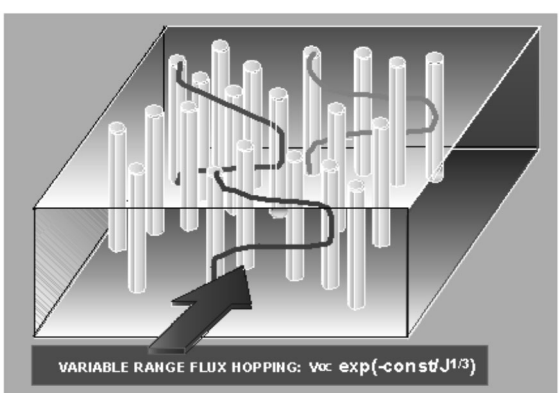

Figure 10. Experimental data for different types of dynamic regimes.

Experimental evidence for Bose-glass behavior in $Bi_2Sr_2CaCu_2O_8$ crystals with columnar defects

M. Konczykowski and N. Chikumoto*
V. M. Vinokur
M. V. Feigelman

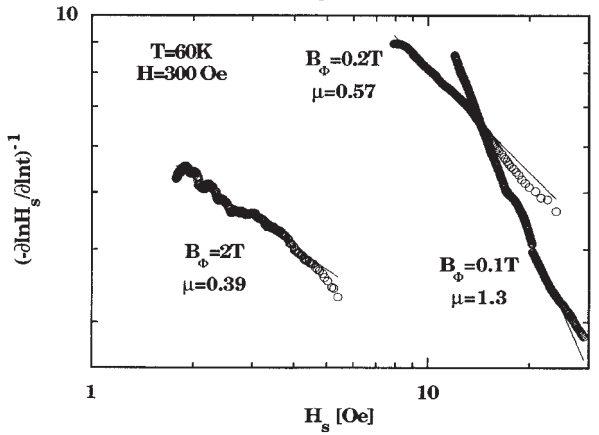

FIG. 4. Energy barrier for flux creep ($1/S$) vs stray field H_s recorded at 300 Oe and 60 K on BSCCO:2212 samples irradiated to various doses.

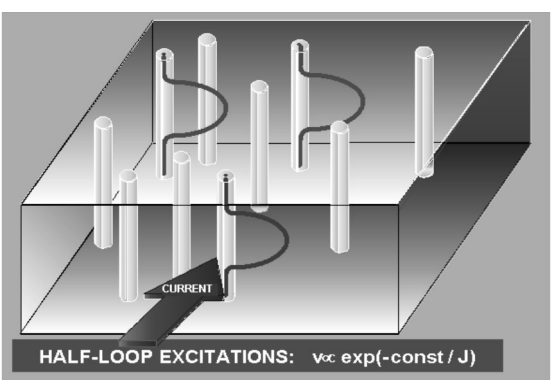

Figure 11. Experimental data for different types of dynamic regimes.

property that we used to derive the nonlinear behavior at small forces was *the elastic nature of the driven object*, i.e. the existence of the internal degrees of freedom. Thus one can draw a conclusion that *any* elastic object in a random environment must exhibit creep-like motion at small forces and low temperatures. Moreover, one can notice next that thermal fluctuations are not the only mechanism that can provide transitions between the low-lying metastable states in the random potential and that *quantum fluctuations* will do the job equally well. We thus arrive at the notion of the *quantum creep*. Such quantum motion of vortices was indeed discovered in high temperature superconductors at very low temperatures where quantum tunnelling of vortices through the barriers separating the energy valleys appeared to be more effective than activation *over* these barriers.

In a more refined language one can say that for any system that can be described by the general energy functional

$$\mathcal{F}[\phi] = \int \mathrm{d}\mathbf{R}\left[\frac{\hat{\mathbf{C}}}{2}\left(\frac{\partial\phi}{\partial\mathbf{R}}\right)^2 + V(\phi,\mathbf{R})\right], \tag{22}$$

where $\hat{\mathbf{C}}$ is the general elastic matrix and ϕ is a general field describing the dynamics in question, and $V[\ldots]$ is the appropriate random potential functional. There is a wealth of the physical systems that fall in the category described by the definition (22) including vortices in superconductors, domain walls, charge density waves in crystals, dislocations in solids, polymers, interacting electrons in metals and semiconductors — and many, many others — for which we expect the nonlinear small force response as

$$v \sim \exp(-\,\mathrm{const}/f^{\mu})\,. \tag{23}$$

Indeed, recently creep motion of exactly this form was experimentally observed for the moving domain walls in magnetic films and dislocations. We thus arrive at the final conclusion that the expression (23) is the generic law of the small force dynamics for all the real (since almost all the real systems contain disorder in one or another form) condensed matter systems.

Acknowledgements

This work was supported by the U.S. Department of Energy Office of Science via contract No. W-31-109-ENG-38.

Bibliography

[1] A. Buzdin, A. Varlamov, *The Superconductivity Passion at the end of the Millenium.*

[2] A. A. Abrikosov, Doklady Akademii Nauk SSSR **85**, 489 (1952).
[3] V. L. Ginzburg, L. D. Landau, Zh. Eksp. Teor. Fiz., **20**, 1064 (1950).
[4] A. I. Larkin, Sov. Phys. JEPT, **31**, 784 (1970)
[5] G. Blatter, M. V . Feigelman, V. B. Geshkenbein, A. I. Larkin, and V. M. Vinokur, Rev. Mod. Phys. **66**, 1125 (1994)
[6] M. V. Feigelman and V. M. Vinokur, Phys. Rev. B **41**, 8986 (1990)
[7] L. B. Ioffe and V. M. Vinokur, J. Phys., **C 20**, 6149 (1987)
[8] D. R. Nelson, Phys. Rev. Lett., **60**, 1973 (1988)
[9] D. R. Nelson and V. M. Vinokur, Phys. Rev. Lett., **68**, 2398 (1992); D. R. Nelson and V. M. Vinokur, Phys. Rev. B **48**, 13 060 (1993)
[10] A. V. Lopatin and V. M. Vinokur, Phys. Rev. Lett., (1994)
[11] R. J. Olsson, W.-K. Kwok, *et al*, Phys. Rev. **B 65**, 104520 (2002); C. van der Beek *et al* Phys. Rev. **B 61**, 4259 (2000); L. Krusin–Elbaum, *et al*, Phys. Rev. Lett. **72**, 1914 (1994)
[12] T. Hwa, D. R. Nelson, P. Le Doussal, and V. M. Vinokur, Phys. Rev. Lett., **71**, 3545 (1993)
[13] A. I. Larkin and V. M. Vinokur, Phys. Rev. Lett., **75**, 4666 (1995)
[14] L. D. Landau and E. M. Lifshits, Quantum Mechanics,

Стимулированный магнитным полем переход сверхпроводник–изолятор в InO и специфика возникающего при этом изолятора

В. Ф. Гантмахер
Институт физики твердого тела РАН, Черноголовка, Московская область, Россия

Подробный анализ экспериментальных данных по переходам сверхпроводник-изолятор (в основном в двух материалах — InO и $Nd_{2-x}Ce_xCuO_{4+y}$) доказывает существование в изоляторе «локализованных пар», т.е. парных корреляций между локализованными электронами на Ферми-уровне.

Литература

1. Эксперимент

InO

1. D. Shahar and Z. Ovadyahu, Phys. Rev. B **46**, 10917 (1992).
2. A.F. Hebard and M.A. Paalanen, PRL **65**, 527 (1990).
3. V.F. Gantmakher, M.V. Golubkov, J. G. S. Lok, and A. K. Geim. ЖЭТФ **82**, 951 (1996).
4. V.F. Gantmakher, M.V. Golubkov, V.T. Dolgopolov, G.E. Tsydynzhapov, and A. A. Shashkin, Письма в ЖЭТФ **68**, 345 (1998); Письма в ЖЭТФ **71**, 160 (2000); Письма в ЖЭТФ **71**, 473 (2000).
5. G. Sambandamurthy, L. W. Engel, A. Johansson, and D. Shahar, cond-mat/0307648

Другие материалы

Ультратонкие пленки (Bi, Be,. . .)

1. Y. Liu *et al*, PRB **47**, 5931 (1993).
2. E. Bielejec and W. Wu, PRL **88**, 206802 (2002).
3. J.A. Chervenak, J.M. Valles, Jr. PRB **61**, R9245 (2000).

a-Mo_xSi_{1-x}
a-MoGe — A. Yazdani and A. Kapitulnik, PRL **74**, 3037 (1995).
$Nd_{2-x}Ce_xCuO_{4+y}$ — S. Tanda *et al*, PRL **69**, 533 (1992).
V.F. Gantmakher *et al*, JETPL **77**, 424 (2003).
TiN_x — T.I. Baturina *et al*, cond-mat/0210250 (2002).

2. Теория

Гранулярность (переход в состояние изолятора гранулированных сверхпроводников) — I.S. Beloborodov and K.B. Efetov, PRL **82**, 3332 (1999).
Скейлинг (рассмотрение в духе теории квантовых переходов, основанное на дуализме бозоны-вихри) — M. P. A. Fisher, PRL **65**, 923 (1990).
Сверхпроводящие флуктуации (вычисление в рамках теории БКШ в первом порядке теории возмущений) — V.M. Galitski and A.I. Larkin, PRB **63**, 174506 (2001).
Численные эксперименты (введение дополнительного притяжения между электронами в рамках модели Андерсона) — B. Srinivasan, G. Beneventi, and D.L. Shepelyansky, PRB **66**, 172506 (2002).

Peculiarities of the impurity states in the narrow-gap lead telluride-based semiconductors

D. Khokhlov
Physics Department, Moscow State University, Moscow, Russia

Abstract. Starting from mid-70's, a great deal of both experimental and theoretical efforts has been attracted to the unexplained puzzle of impurity states arising in the IV–VI narrow-gap cubic semiconductors doped with some of the group III elements, and to the unusual effects observed in these materials. We review the experimental results obtained in the field: mixed valence phenomena, electrical activity of impurity centers, persistent photoconductivity and related effects. Some of the features of these semiconductors have provided the possibility of construction of the far-infrared photodetector with extremely high characteristics. The theoretical models proposed so far to account for the physical picture of the processes involved are discussed.

1. Introduction

Investigation of impurity states in the group III-doped narrow-gap IV–VI semiconductors based on the lead telluride has a long tradition in the former Soviet Union. It has started in early 70's [1] and has been extensively developed since that time. The unusual effects observed in these materials, such as persistent photoconductivity and photomemory — are quite analogous to the features of III–V and II–VI semiconductors with the DX-centers. The microscopic structure of the DX-centers in III–V is well established now both experimentally and theoretically [2, 3].

The origin of impurity states in the group III-doped IV–VI is still under discussion. There is a considerable difference from the effects due to the "classic" DX-centers in the relatively wide-gap III–V's and II–VI's. First of all, in the IV–VI's the same impurity can be either donor or acceptor depending on the specific composition of the semiconductor. The variable electrical activity of the III group impurities leads to the pinning of chemical potential. Beside that, the impurity centers in the IV–VI reveal the negative-U behavior independently on the impurity level position in the energy spectrum, in contrast to the DX-centers in III–V and

II–VI. Finally, the one-electron local states are hydrogen-like in III–V and II–VI, whereas they are mostly deep in IV–VI. These metastable local states play an important role in a range of strong and unusual non-equilibrium effects.

2. Mixed valence and electrical activity

Indium initially acts as a donor in PbTe providing the increase of a free electron concentration n [1], but then the value of n saturates. The saturation on the $n(N_{In})$ dependence corresponds to the Fermi level pinning. Additional doping with other impurities does not affect the Fermi level position E_F. Besides, E_F is not linked to the actual band edges [4–6].

The position of a pinned Fermi level in the energy spectrum can be changed by variation of the group III dopant. In PbTe(Ga) the Fermi level is pinned within the gap, and in PbTe(Tl) — rather deep in the valence band [4], and the group III element acts already as an acceptor. Moreover, even for the same dopant the position of E_F can be changed by variation of the lead telluride-based alloy composition. In the range of $Pb_{1-x}Sn_xTe$(In) solid solutions the pinned Fermi level shifts to the bottom of the conduction band with increasing x, crosses the gap and enters the valence band, acting therefore as an acceptor [7].

3. Theoretical models of impurity states

Indium is expected to reveal an acceptor behavior in IV–VI since it substitutes metal. However it can obviously act both as a donor and as an acceptor. According to the idea proposed in [8], indium reveals a negative-U behavior, i.e. the neutral with respect to the lattice state In^{2+} is unstable and dissolves to the donor and acceptor states: $2In^{2+} \rightarrow In^{+} + In^{3+}$. Polarization of the impurity environment is a reason for this reaction.

The clear microscopic picture of the processes involved has been proposed in [9-12]. Due to high values of a dielectric constant ($\varepsilon \sim 10^3$) and to small effective masses ($m \sim 10^{-2} m_e$) the Coulomb potential of an impurity is effectively screened, and the short-range potential gives the main contribution to the formation of an impurity energy spectrum. The short-range character on a potential allows to use in the calculations the averaged over the Brillouin zone characteristics of the energy bands, which may be most easily calculated using the tight-bind approximation. The theory is based on the idea of a “pra-phase”, where the IV–VI lattice is considered as a cubic lattice with a superimposed doubling potential due to the chemical difference of the group IV and group VI atoms that form the valence bonds constructed from the atomic p-orbitals. Three filled by half bands originating from the overlapping atomic p-orbitals arise in the “pra-phase”. The

doubling potential provides appearance of the gap in the IV–VI spectrum just at the Fermi energy. The real electronic spectrum may be calculated by taking into account the spin-orbital interaction and the overlapping of the p-orbitals of a non-neighboring atoms.

Understanding of the origin of the actual bands in IV–VI gives a key for the solution of the problem of mixed valence of the group III elements. This element replacing the metal atom can exist in three atomic configurations — one-valent s^2p^1, two-valent s^1p^2 and three-valent s^0p^3 [12]. p-electrons participate in the formation of the actual bands, so therefore the element is acceptor in the first case, neutral impurity in the second one, and donor in the third case. Realization of the particular valence of an impurity atom depends on the Fermi level position E_F. When the total energy of the s^0p^3 and the s^2p^1 configurations becomes equal, the Fermi level is pinned. The total energy of the neutral with respect to the lattice s^1p^2 configuration is higher than E_F, thus the impurity effectively reveals the negative-U behavior. The valence switching corresponds to the transfer of electrons from- and to the deep s-shell, therefore the group III element can reveal electrical activity of both donor and acceptor type.

4. Long-term relaxation processes

Most of attention to the group III-doped IV–VI has been attracted due to the long-term relaxation processes observed in these semiconductors at the low temperatures $T \ll T_c$ under the action of different external factors — infrared illumination [13], magnetic field [14], electric field [15]. The value of T_c is about 25 K in the case of indium doping and about 80 K for the gallium impurity. For the In-doped alloys a strong persistent photoresponse is observed at $T < 25$ K independently on whether the Fermi level is pinned in the allowed band or in the gap. This point makes a substantial difference from the case of the DX-centers in III–V's, where the persistent photoconductivity is observed only when the DX-level lies in the gap [2].

Kinetics of the persistent photoconductivity decay is also unusual. Two parts of the photoconductivity relaxation are observed: the fast part is followed by the slow one [4–6]. The characteristic time τ of the fast process is (1 ms–1 s) whereas for the slow part τ may exceed 10^5 s at the low temperatures. The value of τ for both processes only slightly depends on the temperature when $T \ll T_c$ indicating a non-activation mechanism of relaxation. One more argument in support of this statement is the non-exponential character of both fast and slow relaxation. The rate of the slow relaxation process depends on the history of preceding photoexcitation [5].

5. Local metastable states

The experimental data clearly show that the processes involved cannot be explained if one takes into account only one local state providing the Fermi level pinning. Indeed, observation of two parts of the relaxation curve give a direct indication for the existence of at least two different local states in the energy spectrum of the semiconductor.

In the case of the group III-doped IV–VI's the excited local states are separated by a potential barriers from both ground impurity states and the extended electron states, in contrast to the situation with the DX-centers in III–V's where the excited local states there are shallow. Metastability of the excited local electron states results in an appearance of a range of unusual effects not observed in materials with the "classic" DX-centers.

The giant negative magnetoresistance with an amplitude exceeding 10^6 in some cases has been observed in $Pb_{0.75}Sn_{0.25}Te(In)$ where the Fermi level is pinned in the gap [16]. The explanation proposed in [16] assumes trapping of the injected electrons on the metastable one-electron impurity states $E_1(s^1p^2)$. Application of a magnetic field pushes the E_1 states above the conduction band bottom thus providing electron delocalization.

The idea developed in [12] allows to propose the alternative origin of impurity states responsible for the giant negative magnetoresistance effect. The empty impurity centers (s^0p^3) give rise to a short-range attractive potential that in turn provides splitting of an impurity $(p\text{-like})$ state from the conduction band bottom. Electron localized in this state can have a somewhat different g-factor compared to the conduction band electrons. Therefore application of the magnetic field may push the electrons trapped on this level into the conduction band.

This idea has been further developed in [17] to account for appearance of the long-term non-equilibrium effects at low temperatures. According to this idea, the metastable one-electron impurity states $E_1(s^1p^2)$ lie rather high in the conduction band. The two-electron excitation is forbidden in the first approximation, therefore the transfer of excited electrons from the extended to the ground two-electron local state can proceed only through the one-electron metastable local state. So trapping of excited electrons to the ground state goes in two steps: first one electron must localize on an impurity center, and only after that this center can trap a second electron and transfer to the ground state. The first step implies increase in the center energy, therefore an effective barrier is formed between the ground state and the extended electron state. One can see that no considerable lattice relaxation is needed in this mechanism.

Application of a strong and short $(< 10\mu s)$ microwave pulses to the

$Pb_{1-x}Sn_xTe(In)$ samples results in a complete quenching of the persistent photoresponse [18]. Moreover, if the persistent photoconductivity is quenched by the microwave pulses of a minimal necessary power, the quantum efficiency η of a material increases up to $\sim 10^2$, whereas out of this regime $\eta \sim 1$. Application of the short microwave pulse leads to the localization of electrons to the metastable local state. Some of the metastable centers may form a cluster with strong internal interaction. Excitation of one electron from this cluster leads to the avalanche excitation of other centers providing the increase of a quantum efficiency.

6. New type of the far-infrared photodetectors

Unusual features of the group III-doped lead telluride-based alloys have provided the possibility of construction of the sensitive far-infrared radiometer. The persistent photoresponse in combination with the possibility of fast resetting of an accumulated signal together with the quantum efficiency stimulation provides a giant increment in the signal-to-noise ratio and in a current responsivity of a photodetector. This approach has been realized in [19]. Despite the measurement technique was far from being sensitive (the lowest detectable current only 10^{-7} A) the photon flux of 10^5 ph/s and the power of 10^{-16} W at $\lambda = 18\mu$m have been detected for the operating rate of 3 Hz, the current responsivity was no less than 10^9 A/W. Application of a more advanced measurement technique would definitely improve the NEP value.

Direct comparison of performance of the state of the art Si(Sb) and Ge(Ga) far-infrared photodetectors with a photodetector based on $Pb_{1-x}Sn_xTe(In)$ has been performed in [20, 21]. In these experiments, the same cryogenics and readout electronics has been used for both doped group-IV photodetectors and the $Pb_{1-x}Sn_xTe(In)$ sample. It has been shown that the responsivity of the $Pb_{1-x}Sn_xTe(In)$ photodetector is by 3–7 orders of magnitude higher than for its doped group-IV counterparts, depending on the operating wavelength. Strong persistent photoresponse has been observed in $Pb_{0.75}Sn_{0.25}Te(In)$ at the wavelengths of 90, 116 μm [20] and 176, 241 μm [21]. These wavelengths correspond to the radiation quantum energy, that is considerably lower than the ground impurity state activation energy. It means that the metastable impurity states are responsible for this photoresponse. The cut-off wavelength of this photoresponse is at least higher than 241 μm that is the highest red cut-off wavelength observed so far for the quantum detectors of radiation. It is likely that the operating range of the $Pb_{1-x}Sn_xTe(In)$-based photodetectors covers the whole submillimeter region.

The group III-doped lead telluride-based photodetectors have extremely high radiation hardness $\sim 10^{17}$ cm^{-2} [22]. This value is by 10^4 times higher than for

the other far-infrared photodetectors.

Specifics of impurity states makes very easy the construction of a focal-plane array on $Pb_{1-x}Sn_xTe(In)$. The local infrared illumination leads to the local generation of the nonequilibrium free electrons [23]. So one may construct the focal plane array in which the signal is internally integrated by every effective element. There exists an idea of a simple information readout [19].

Summary

Doping of the lead telluride-based alloys with some of the group III impurities, such as indium or gallium, results in an appearance of the unusual impurity states in these narrow-gap IV–VI semiconductors. In contrary to the DX-centers in III–V's and II–VI's the impurity centers in IV–VI exhibit the negative-U behavior independently on the position of a DX-level in the semiconductor energy spectrum. Another circumstance of a crucial importance is existence of a barrier between excited one-electron local impurity state and both ground two-electron local state and state of an electron in the conduction band. Presence of these barriers results in an appearance of a range of unusual non-equilibrium effects that are absent in the case of "classical" DX-centers, where the one-electron local states are shallow.

Acknowledgments

The research described in this paper was supported in part by the RFBR grant 02-02-17057 by the Russian Federation President Grant Council grant NS-1786.2003.2 and by the INTAS grant 2001-0184.

Bibliography

[1] V. I. Kaidanov, R. B. Mel'nik and I. A. Chernik, Sov. Phys. Semicond. **7**, 522 (1973).
[2] P. M. Mooney, J. Appl. Phys. **67**, R1 (1990).
[3] D. J. Chadi and K. J. Chang, Phys. Rev. Letters **61**, 7 (1988).
[4] V. I. Kaidanov and Yu. I. Ravich, Sov. Phys. Uspekhi **28**, 31 (1985).
[5] B. A. Akimov, A. V. Dmitriev, L. I. Ryabova and D. R. Khokhlov, Phys. Stat. Sol. (a) **137**, 9 (1993).
[6] B. A. Volkov, L. I. Ryabova and D. R. Khokhlov, Physics-Uspekhi **45**, 819 (2002).
[7] B. A. Akimov, L. I. Ryabova, S. M. Chudinov and O. B. Yatsenko, Sov. Phys. Semicond. **13**, 759 (1979).
[8] I. A. Drabkin and B. Ya. Moizhes, Sov. Phys. Semicond. **17**, 611 (1983).
[9] B. A. Volkov and O. A. Pankratov, Sov. Phys. Dokl. **25**, 922 (1980).
[10] B. A. Volkov and O. A. Pankratov, Sov. Phys. JETP **61**, 164 (1985).
[11] O. A. Pankratov and B. A. Volkov. Soviet Scientific Reviews A (Physics) **9**, 355 (1987).
[12] B. A. Volkov and O. M. Ruchaiskii, Sov. Phys. JETP Lett. **62** 217 (1995).

[13] B. M. Vul, I. D. Voronova, G. A. Kaluzhnaya, T. S. Mamedov and T. Sh. Ragimova, Pis'ma v Zhurn. Eksp. Teor. Fiz. **29**, 21 (1979).
[14] B. A. Akimov, N. B. Brandt, S. A. Bogoslovskiy, L. I. Ryabova and S. M. Chudinov, Pis'ma v Zhurn. Eksp. Teor. Fiz. **29**, 11 (1979).
[15] B. A. Akimov, N. B. Brandt, B. S. Kerner, V. N. Nikiforov and S. M. Chudinov, Solid State Commun. **43**, 31 (1982).
[16] B. A. Akimov, A. V. Nikorich, D. R. Khokhlov and S. N. Chesnokov, Sov. Phys. Semicond. **23**, 418 (1989).
[17] A. I. Belogorokhov, B. A. Volkov, I. I. Ivanchik and D. R. Khokhlov, JETP Lett. **72**, 123 (2000).
[18] B. A. Akimov and D. R. Khokhlov, Sem. Sci. Technol. **8**, S349 (1993).
[19] S. N. Chesnokov, D. E. Dolzhenko, I. I. Ivanchik and D. R. Khokhlov, Infrared Phys. **35**, 23 (1994).
[20] D. R. Khokhlov, I. I. Ivanchik, S. N. Raines, D. M. Watson and J. L. Pipher, Appl. Phys. Lett., **76**, 2835 (2000).
[21] K. G. Kristovskii, A. E. Kozhanov, D. E. Dolzhenko, I. I. Ivanchik, D. Watson and D. R. Khokhlov, Physics-Solid State **46**, 122 (2004).
[22] E. P. Skipetrov, A. N. Nekrasova and A. G. Khorosh, Semiconductors **28**, 478 (1994).
[23] B. A. Akimov, N. B. Brandt, S. N. Chesnokov, K. N. Egorov and D. R. Khokhlov, Solid State Commun. **66**, 811 (1988).

«Металлическая» проводимость, переход металл–диэлектрик и сопуствующие явления в двумерной электронной жидкости

В. М. Пудалов
Физический институт им. П. Н. Лебедева РАН, Москва, Россия

Две лекции на названную тему являются введением в сравнительно молодую область исследования свойств сильно-коррелированных и разупорядоченных двумерных систем заряженных фермионов. Будут рассмотрены результаты экспериментальных исследований проводимости, магнитосопротивления, спиновой восприимчивости, спиновой намагниченности и эффективной массы, перенормированных межэлектронным взаимодействием и беспорядком.

План лекций

1. Моттовская полуклассическая картина перехода металл–диэлектрик.

2. Квантовый транспорт заряда в отсутствии магнитного поля.
2.1. Транспорт по делокализованным состояниям: диффузионный и баллистический режимы.
2.2. Транспорт по локализованным состояниям.
2.3. Фазовая когерентность и транспорт.
2.4. Подавление слабой локализзации в перпендикулярном магнитном поле.
2.5. Одночастичная скейлинговая теория локализации.
3. Переход металл–диэлектрик в 2D.
3.1. Повторяющиеся переходы между состояниями: (жидким) с квантованным Холловским сопротивлением и изолятора (твердым) в перпендикулярном поле.
3.2. «Всплывание» протяженных состояний и их слияние друг с другом.
3.3. Переход металл–диэлектрик в нулевом поле (электронная жидкость–вигнеровский кристалл?)
3.4. Коллективный характер транспорта в твердом состоянии.
4. Количественное изучение электрон-электронного взаимодействия в 2D.
4.1. Экспериментальный метод: Интерференция квантовых осцилляций в «скрещенных» магнитных полях.
4.2. Термодинамическое измерение спиновой намагниченности.
4.3. Ферми-жидкостная перенормировка параметров в 2D электронной жидкости:
— эффективная масса
— спиновая восприимчивость
— сжимаемость электронной жидкости.
4.4. Описание металлически-подобного транспорта с помощью измеренных ферми-жидкостных параметров.
4.5. Сопоставление результатов измерений на различных 2D системах.
5. Сравнение эксперимента с теорией вдали от критического режима (при высокой проводимости, $\sigma \gg e^2/h$).
6. Сопоставление эксперимента с теорией в критическом режиме ($\sigma \ll e^2/h$).
7. Транспорт в присутствии магнитного поля в 2D плоскости.
8. Еще не решенные проблемы.

Электростатические модели фазовых переходов металл–изолятор в кристаллах Ge и Si с водородоподобными примесями

Н. А. Поклонский

Белорусский государственный университет, Минск, Республика Беларусь

В лекции излагаются результаты расчета параметров концентрационных фазовых переходов изолятор–металл и металл–изолятор в пределе нулевой температуры ($T \to 0$).

1. На изоляторной стороне перехода изолятор–металл при увеличении концентрации N легирующей примеси вплоть до критической концентрации N_c происходит неограниченное возрастание статической относительной диэлектрической проницаемости $\varepsilon_r(N)$ кристаллического образца [1–3]. Для определенности рассмотрим кристаллический полупроводник *n*-типа с концентрацией доноров $N = N_0 + N_{+1}$ в зарядовых состояниях (0) и (+1) и акцепторов в зарядовом состоянии (-1) с концентрацией $N_{-1} = KN$, где K — степень компенсации доноров. Условие электронейтральности: $N_{+1} = KN$.

По модели [4, 5] с учетом поляризуемости как атомов кристаллической матрицы, так и электрически нейтральных доноров, критическая концентрация N_c для перехода изолятор–металл и зависимость $\varepsilon_r(N)$ от концентрации доноров N на изоляторной стороне имеют вид:

$$N_c^{1/3} a_H = \frac{0.542}{[(1-K)(\varepsilon_r+2)]^{1/3}}, \quad \varepsilon_r(N) = \frac{\varepsilon_r + 2N/N_c}{1 - N/N_c}, \qquad (1)$$

где $a_H = e^2/8\pi\varepsilon_r\varepsilon_0 I_{d(a)}$ — радиус орбиты электрона (дырки) одиночного водородоподобного донора (акцептора) с энергией ионизации $I_{d(a)}$ в кристаллической решетке с диэлектрической проницаемостью $\varepsilon_r\varepsilon_0$; e — заряд электрона; $K \ll 1$; $\varepsilon_r(N \to 0) = \varepsilon_r$.

Расчет зависимости $\varepsilon_r(N)$ по формуле 1 для кристаллов кремния показан в сравнении с экспериментальными данными на рис. 1. При обработке экспериментальных данных [1, 3, 6, 7] использовались средние значения критических концентраций примесей для $K \to 0$ (см. табл. 1): $N_c(\text{Si:As}) = 7.8 \cdot 10^{18}$ см$^{-3}$, $N_c(\text{Si:P}) = 3.8 \cdot 10^{18}$ см$^{-3}$, $N_c(\text{Si:B}) = 4.1 \cdot 10^{18}$ см$^{-3}$.

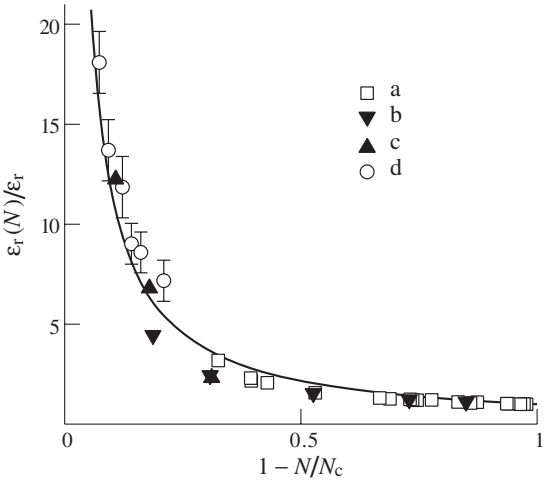

Рис. 1. Зависимость макроскопической относительной диэлектрической проницаемости $\varepsilon_r(N)$ слабо компенсированного кремния от концентрации N основных легирующих примесей. Точки — экспериментальные данные: *a* — *n*-Si:As [1], *b* — *n*-Si:P [6], *c* — *n*-Si:P [7], *d* — *p*-Si:B [3]. Кривая — расчет $\varepsilon_r(N)$ по 1 при $K = 0$ и $\varepsilon_r = 11.5$

Таблица 1. Экспериментальные значения критической концентрации N_c примеси в кристаллах Si при разных степенях компенсации K

Параметры кристалла, электронов (n) и дырок (p) [8, 9]	Легированный полупроводник	$I_{d(a)}$, мэВ [8, 9]	N_c, см$^{-3}$	K	Источник
1	2	3	4	5	6
Si	*n*-Si:As	53.8	$7.8{\cdot}10^{18}$	< 0.01	[10]
$\varepsilon_r = 11.5$	*n*-Si:P	45.6	$3.48{\cdot}10^{18}$	< 0.01	[11]
$m_n = 0.322m_0$			$3.7{\cdot}10^{18}$	< 0.01	[12]
$\nu_n = 6$			$(4.15 \pm 0.2){\cdot}10^{18}$	< 0.01	[13]
$m_p = 0.591m_0$			$(4.74 \pm 0.5){\cdot}10^{18}$	0.15 ± 0.05	
$\nu_p = 1$			$(6.77 \pm 0.8){\cdot}10^{18}$	0.37 ± 0.05	
			$(1.2 \pm 0.2){\cdot}10^{19}$	0.54 ± 0.05	
	n-Si:Sb	42.7	$2.9{\cdot}10^{18}$	< 0.01	[14]
	p-Si:B	44.4	$4.1{\cdot}10^{18}$	< 0.01	[15]

2. С металлической стороны переход металл–диэлектрик экспериментально наблюдается как неограниченный рост электрического сопротивления на постоянном токе при уменьшении концентрации N примеси вплоть до N_c или при увеличении ее степени компенсации.

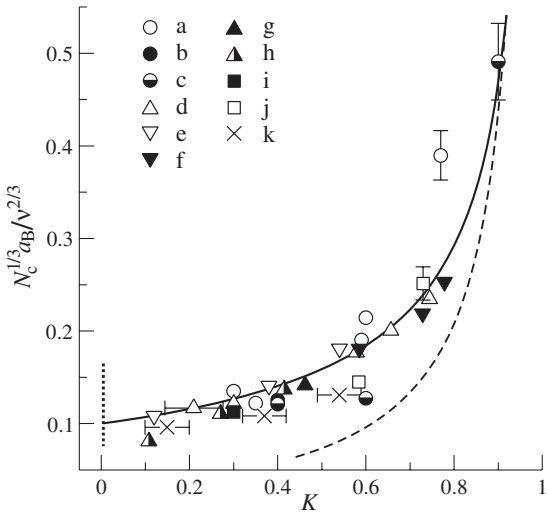

Рис. 2. Зависимость критической концентрации N_c доноров (акцепторов) в Ge и Si от степени их компенсации K. Точки — экспериментальные данные: *a* — *p*-Ge:Ga [27–29], *b* — *p*-Ge:Ga [21], *c* — *p*- Ge:Ga [30], *d* — *n*-Ge:As [23, 27, 31], *e* — *n*- Ge:As [22], *f* — *n*-Ge:As [24], *g* — *n*-Ge:Sb [24], *h* — *n*- Ge:Sb [23], *i* — *n*-Ge:Sb [32], *j* — *n*-Ge:P [23, 27], *k* — *n*-Si:P [13]. Сплошная линия — расчет по 3; штриховая линия — расчет по модели [17]. (Пунктиром при $K = 0.01$ показан диапазон экспериментальных данных по N_c из работ [10–15, 18–26], представленных в табл. 1 и 2, со средним значением $N_c^{1/3}a_B/\nu^{2/3} = 0.1$)

Предполагается, что флуктуации электростатической энергии, создаваемые в кристалле ионами примесей и электронами проводимости, имеют гауссово (нормальное) распределение с дисперсией W^2. Из условия равенства уровня протекания (порога подвижности) E_μ уровню Ферми E_F, зависимость критической для перехода металл–изолятор концентрации N_c примеси от степени ее компенсации K при температуре $T \to 0$ можно получить [4, 5, 16] в виде (ср. [17]):

$$N_c^{1/3}a_B = 0.238\left(\frac{W}{E_B}\right)^{1/2}\left[\frac{\nu}{1-K}\int_{-\infty}^{E_\mu/W}\left(\frac{E_\mu}{W}-x\right)^{3/2}\exp\left(\frac{-x^2}{2}\right)\mathrm{d}x\right]^{1/3}, \quad (2)$$

где $a_B = 4\pi\varepsilon_r\varepsilon_0\hbar^2/me^2$, $E_B = e^2/8\pi\varepsilon_r\varepsilon_0 a_B$ — боровские радиус[1] и энергия; ν — число долин в разрешенной для основных носителей заряда энергетиче-

[1]Для кристаллов Ge и Si как *n*-, так и *p*-типа $a_H \neq a_B$. Ясно, что для атома водорода в вакууме $\varepsilon_r = 1$, $m = m_0$ и $a_H = a_B$.

Таблица 2. Критическая концентрация N_c примеси в кристаллах Ge при разных степенях компенсации K (номера в названиях столбцов соответствуют табл. 1)

1	2	3	4	5	6
Ge $\varepsilon_r = 15.4$ $m_n = 0.22m_0$ $\nu_n = 4$ $m_p = 0.38m_0$ $\nu_p = 1$	*n*-Ge:As	14.2 мэВ	$3{\cdot}10^{17}$ см$^{-3}$	$K < 0.01$	[18]
			$3.5{\cdot}10^{17}$	< 0.01	[19, 20]
			$(3.5 \pm 0.18){\cdot}10^{17}$	< 0.01	[22]
			$(4 \pm 0.2){\cdot}10^{17}$	$K = 0.12$	
			$(8.8 \pm 0.2){\cdot}10^{17}$	0.38	
			$(1.87 \pm 0.9){\cdot}10^{18}$	0.54	
			$3.83{\cdot}10^{17}$	< 0.01	[23]
			$(5 \pm 1){\cdot}10^{17}$	0.21 ± 0.07	[27]
			$5.64{\cdot}10^{17}$	0.3	[31]
			$1.86{\cdot}10^{18}$	0.58	[24]
			$3.3{\cdot}10^{18}$	0.73	
			$5.1{\cdot}10^{18}$	0.78	
	n-Ge:P	12.88	$2.5{\cdot}10^{17}$	< 0.01	[19, 20]
			$2.56{\cdot}10^{17}$	< 0.01	[23]
			$(5 \pm 1){\cdot}10^{18}$	0.73	[27]
	n-Ge:Sb	10.45	$1.5{\cdot}10^{17}$	< 0.01	[18]
			$1.53{\cdot}10^{17}$	< 0.01	[23]
			$1.68{\cdot}10^{17}$	< 0.01	[25]
			$2{\cdot}10^{17}$	< 0.01	[24]
			$8.9{\cdot}10^{17}$	0.46	
			$4.5{\cdot}10^{17}$	0.3	[32]
	p-Ge:Ga	11.32	10^{17}	< 0.01	[21]
			$2{\cdot}10^{17}$	0.4	
			$1.13{\cdot}10^{17}$	< 0.01	[23]
			$1.86{\cdot}10^{17}$	< 0.01	[26]
			$2.5{\cdot}10^{17}$	0.3	[28]
			$1.85{\cdot}10^{17}$	0.35	[29]
			$(1.8 \pm 0.3){\cdot}10^{17}$	0.4	[30]
			$(2.1 \pm 0.3){\cdot}10^{17}$	0.6	
			$(1.2 \pm 0.3){\cdot}10^{19}$	0.9	
			$(7 \pm 1){\cdot}10^{17}$	0.59 ± 0.02	[27]
			$(1 \pm 0.2){\cdot}10^{18}$	0.6 ± 0.02	
			$(6 \pm 1){\cdot}10^{18}$	0.77 ± 0.02	

ской зоне ($\nu_n = 4$ для *n*-Ge, $\nu_n = 6$ для *n*-Si; $\nu_p = 1$ для *p*-Ge и *p*-Si); m — эффективная масса электрона (дырки) в одной долине.

В модели [4, 16] величина $W = W_{nn} \approx 1.64(e^2/4\pi\varepsilon_r\varepsilon_0)(8\pi N_c/3)^{1/3}$ обусловлена кулоновским взаимодействием только ближайших зарядов (ионов примесей с концентрацией $(1 + K)N_c$ и электронов проводимости с концен-

трацией $n_c = (1 - K)N_c$). Значение $E_\mu/W_{nn} = -1.15$ находится согласованием 2 с экспериментальными данными [10–15, 18–26] для некомпенсированных кристаллов: $[N_c(K \to 0)]^{1/3} a_B/\nu^{2/3} = 0.1$ (см. табл. 1, 2). Если принять, что отношение E_μ/W_{nn} равно -1.15 для $0 < K < 1$, то из 2 следует зависимость $N_c(K)$ для перехода металл–изолятор в виде (сплошная линия на рис. 2):

$$\frac{N_c^{1/3} a_B}{\nu^{2/3}} = \frac{0.1}{(1-K)^{2/3}}. \tag{3}$$

В модели [17] величина $W = W_s = (e^2/4\sqrt{2}\pi\varepsilon_r\varepsilon_0)(1+K)^{2/3}[N_c/(1-K)]^{1/3}$ обусловлена экранированием электронами (или дырками) флуктуаций концентрации ионов примесей. Полагая, что критическая доля объема полупроводника, содержащая электроны и соответствующая уровню их протекания, равна 0.17, имеем $E_\mu/W_s = -0.675\sqrt{2}$. Расчет $N_c(K)$ по модели [17] с учетом формулы 2 при $W = W_s$ показан на рис. 2 штриховой линией.

Литература

[1] T. G. Castner. Phil. Mag. B **42** (6) 873–893 (1980).
[2] T. G. Castner, N. K. Lee, H. S. Tan, L. Moberly, O. Symko. J. Low Temp. Phys. **38** (3-4) 447–473 (1980).
[3] M. Lee, J. G. Massey, V. L. Nguyen, B. I. Shklovskii. Phys. Rev. B **60** (3) 1582–1591 (1999).
[4] Н. А. Поклонский, А. И. Сягло. ФТТ **40** (1) 147–151 (1998).
[5] Н. А. Поклонский, С. А. Вырко, А. Г. Забродский. ФТТ **46** (6) (2004).
[6] M. Capizzi, G. A. Thomas, F. DeRosa, R. N. Bhatt, T. M. Rice. Phys. Rev. Lett. **44** (15) 1019–1022 (1980).
[7] H. F. Hess, K. DeConde, T. F. Rosenbaum, G. A. Thomas. Phys. Rev. B **25** (8) 5578–5580 (1982).
[8] *Semiconductors — Basic data*, ed. by O. Madelung (Berlin, Springer, 1996).
[9] *Handbook series on semiconductor parameters*, ed. by M. Levinstein, S. Rumyantsev, M. Shur (Singapore, World Scientific, 1996) v. 1; (Singapore, World Scientific, 1999) v. 2.
[10] P. F. Newman, D. F. Holcomb. Phys. Rev. B **28** (2) 638– 640 (1983).
[11] P. Dai, Y. Zhang, M. P. Sarachik. Phys. Rev. B **49** (19) 14039–14042 (1994).
[12] G. A. Thomas, M. Paalanen, T. F. Rosenbaum. Phys. Rev. B **27** (6) 3897–3900 (1983).
[13] U. Thomanschefsky, D. F. Holcomb. Phys. Rev. B **45** (23) 13356–13362 (1992).
[14] A. P. Long, H. V. Myron, M. Pepper. J. Phys. C **17** (17) L425–L432 (1984).
[15] P. Dai, S. Bogdanovich, Y. Zhang, M. P. Sarachik. Phys. Rev. B **52** (16) 12439–12440 (1995).
[16] Н. А. Поклонский, С. А. Вырко. Журн. прикл. спектр. **69** (3) 375–382 (2002).

[17] B. I. Shklovskii, A. L. Efros. *Electronic properties of doped semiconductors* (Berlin, Springer, 1984).
[18] А. Т. Лончаков, Г. А. Матвеев, И. М. Цидильковский. ФТП **22** (8) 1396–1400 (1988).
[19] P. P. Edwards, M. J. Sienko. Phys. Rev. B **17** (6) 2575- -2581 (1978).
[20] M. N. Alexander, D. F. Holcomb. Rev. Mod. Phys. **40** (4) 815–829 (1968).
[21] H. Fritzsche. Phil. Mag. B **42** (6) 835–844 (1980).
[22] R. Rentzsch, M. Müller, Ch. Reich, B. Sandow, A. N. Ionov, P. Fozooni, M. J. Lea, V. Ginodman, I. Shlimak. Phys. Stat. Sol. (b) **218** (1) 233–236 (2000).
[23] А. Г. Забродский, М. В. Алексеенко, А. Г. Андреев, М. П. Тимофеев. *Тез. докл. 25-го Всесоюзн. совещ. по физике низких температур* (Ленинград, 1988) ч. 3, с. 60–61.
[24] W. Sasaki, C. Yamanouchi. Journal of Non-Crystalline Solids **4** 183–191 (1970).
[25] S. B. Field, T. F. Rosenbaum. Phys. Rev. Lett. **55** (5) 522–524 (1985).
[26] K. M. Itoh. Phys. Stat. Sol. (b) **218** (1) 211–216 (2000).
[27] А. Г. Забродский. ФТП **14** (8) 1492–1498 (1980).
[28] A. G. Zabrodskii, A. G. Andreev. Int. J. Mod. Phys. B **8** (7) 883–889 (1994).
[29] A. G. Zabrodskii, A. G. Andreev, S. V. Egorov. Phys. Stat. Sol. (b) **205** (1) 61–68 (1998).
[30] R. Rentzsch, O. Chiatti, M. Müller, A. N. Ionov. Phys. Stat. Sol. (b) **230** (1) 237–241 (2002).
[31] А. Г. Забродский, К. Н. Зиновьева. ЖЭТФ **86** (2) 727–742 (1984).
[32] F. R. Allen, R. H. Wallis, C. J. Adkins. *Proc. 5th Int. Conf. Amorphous and liquid semiconductors (Garmisch–Partenkirchen, 1973)*, ed. by J. Stuke, W. Brening (London, Taylor & Francis, 1974) v. 2, p. 895–900.

Many-body effects in hopping conduction

M. Pollak
Dept. of Physics UC Riverside, USA

The talk will overview the current understanding of hopping conduction in the presence of Coulomb interaction. It has been known for three decades that Coulomb interaction have a profound effect on hopping transport in strongly disordered semiconductors. The important reason for it is the drastic modification of the density of states by the interactions. A large number of experiments bear out a single particle transport theory by Efros and Shklovskii, at least as far as the functional dependence of the conductivity on temperature is concerning. On the other hand, it has been somewhat of a mystery why many-body effects (to be discussed) should be negligible in a strongly interaction system. Relatively recently, carefully done experiments detected substantial quantitative deviation from the Efros–Shklovskii theory and they were attributed to many-body effects. Different types of recent sophisticated computer simulations gave incompatible results. I shall discuss these theories how experiments relate to them and possible reasons for disagreements.

Наноалмазы. Нерешенные проблемы

А. Я. Вуль
Физико-технический институт им. А. Ф. Иоффе РАН, С.-Петербург, Россия

Наноалмазами называют углеродные кластеры с характерными размерами области когерентного рассеяния рентгеновских лучей менее 10 нм. Наноалмазы природного происхождения были обнаружены в космических объектах [1, 2], кристаллиты с такими характерными размерами образуются при определенных параметрах синтеза CVD алмазных пленок [3, 4], однако большинство исследований направлено на изучение свойств, так называемых детонационных наноалмазов, получаемых непосредственно из углерода взрывчатых веществ при детонации в замкнутом объеме [5, 6]. Детонационный метод был разработан в СССР, и в настоящее время производство наноалмазов этим методом в России, Украине и Белоруссии осуществляется в промышленных

масштабах. Несмотря на освоение в производстве, ряд принципиальных вопросов физических и физико-химических свойств наноалмазов остается неясными.

В лекции будут рассмотрены следующие вопросы:
— агрегация алмазных нанокластеров,
— стабильность наноалмазов,
— интеркаллирование наноалмазов металлами,
— структурные фазовые переходы наноалмаз–луковичная форма углерода–нанографит.

Литература

[1] R. S. Lewis, M. Tang, J. G. Wackler, E. Anders, E. Steel. *Interstellar diamond in meteorites*. Nature, **326**, 160 (1987).

[2] Z. R. Dai, J. P. Bradley, D. J. Joswiak, D. E. Brownlee, H. G. G. Hill, M. J. Genge. *Possible in situ formation of meteoritic nanodiamonds in the early solar system*. Nature, **418**, 157 (2002).

[3] J. Birrel, J. A. Carlisle, O. Auciello, D. M. Gruen, J. M. Gibson. *Morphology and electronic structure in nitrogen-doped ultrananocrystalline diamond*. Appl. Phys. Lett., **81**, 2235 (2002).

[4] J. Phillip, P. Hess, T. Feygelson, J. E. Butler, S. Chattopadhyay, K. H. Chen, L. C. Chen. *Elastic, mechanical and thermal properties of nanocrystalline diamond films*. J. Appl. Phys., **93**, 2164 (2003).

[5] В. Ю. Долматов. *Ультрадисперсные алмазы детонационного синтеза. Получение, свойства, применения*. (СПб., Изд-во СПбГПУ), 344 с. (2003).

[6] В. В. Даниленко. *Синтез и спекание алмаза взрывом*. (Москва, Энергоатомиздат), 272 с. (2003).

Магнитный углерод

Т. Л. Макарова

Физико-технический институт им. А. Ф. Иоффе РАН, С.-Петербург, Россия

Ромбоэдрическая фаза полимеризованного фуллерена C_{60} ведет себя как типичный ферромагнетик: имеется гистерезис в петлях намагничивания: насыщение намагниченности, точка Кюри при 500 К. После того, как первоначальные результаты были повторены в нескольких группах, а также было визуализировано движение доменных стенок в беспримесном образце по-

лимеризованного фуллерена, стало очевидно, что ферромагнетизм является свойством, присущим самому углероду.

В докладе рассматриваются экспериментальные факты, полученные в течение трех последних лет, а также теоретическое обоснование магнетизма углерода.

Лазер на свободных электронах и метрология гиговатных импульсных потоков ВУФ излучения

С. В. Бобашев

Физико-технический институт им. А. Ф. Иоффе РАН, С.-Петербург, Россия

Приводятся описание и параметры нового источника интенсивных импульсных потоков вакуумного ультрафиолетового излучения. Источником служит лазер на свободных электронах, созданный в Германии (VUV-FEL at the TESLA facility in Hamburg), первая очередь которого продемонстрировала успешную работу в 2002 году.

Рассматриваются методы и устройства для обеспечения высокоточных измерений параметров фотонного пучка. Для абсолютных измерений интенсивных потоков фотонов в вакуумной ультрафиолетовой и мягкой рентгеновской областях спектра разработан в ФТИ оригинальный газовый детектор-монитор. Работа прибора базируется на данных по фотоионизации инертных газов при давлениях, когда наблюдается линейная зависимость выхода фотоинов при взаимодействии интенсивных потоках излучения с газом. Абсолютные сечения фотоионизации инертных газов (с точностью $\pm 3\%$) получены при тщательном анализе надежных экспериментальных измерений абсолютных сечений с учетом предыдущих рекомендации. Существенные уточнения величин сечений в некоторых спектральных областях были получены путем сравнения сечений ионизации инертных газов фотонами и электронами. Прибор является первичным стандартом, практически прозрачным для излучения и не подвергающимся со временем деградации при высоких радиационных нагрузках в отличие от вторичных стандартов, используемым в метрологии радиационных потоков. С помощью детектора-монитора проведены первые измерения интенсивности и временной структуры импульсного излучения ВУФ лазера на свободных электронах с пиковой мощностью более 100 МВт и длительно-

стью импульса 0.1 пс.

Обсуждаются новые направления исследований в области физики взаимодействия интенсивных потоков вакуумного ультрафиолетового и рентгеновского излучения с веществом. Перспективы таких исследований связывают с прогрессом в ускорительной технике и созданием лазеров на свободных электронах, способных генерировать потоки фотонов в рентгеновской области спектра высокой интенсивности.

Шум $1/f$ в полупроводниках и полупроводниковых приборах

М. Е. Левинштейн

Физико-технический институт им. А. Ф. Иоффе РАН, С.-Петербург, Россия

Значение любой измеряемой величины флуктуирует («шумит») либо в силу физической природы этой величины, либо в силу неизбежных погрешностей измерения.

В механических системах амплитуда изучаемых шумов лежит в пределах от 10^{-8} см (физиологи уверяют, что такова амплитуда колебаний мембраны внутреннего уха, соответствующая порогу слышимости) до $\sim 10^{11}$ см (флуктуации диаметра солнца, размер протуберанцев). Частота колебаний лежит в пределах от 10^{-4} до $\sim 10^{7}$ Гц.

В «электрических» системах относительная амплитуда случайных колебаний тока (напряжения) $\delta I/I$ колеблется в пределах от 10^{-11} (атомные стандарты частоты) до 1 («динамический хаос»). Обычно изучаемый частотный диапазон лежит в пределах от 10^{-4} до $\sim 10^{11}$ Гц.

Одной из самых важных характеристик шума является *спектральная плотность шума*. Если, например, измеряются флуктуации напряжения на образце δV, спектральная плотность флуктуаций напряжения $S_v(f)$ (*измеряется* в V^2/Гц) показывает, какая шумовая мощность сосредоточена в полосе 1 Гц на данной частоте f.

Рис. 1 показывает частотную зависимость спектральной плотности шума для двух предельных случаев: музыкального звука («шум» сосредоточен на частоте звука и нескольких гармониках) и «белого» шума — S_v не зависит от частоты в очень широких пределах.

В сотнях объектов самого различного происхождения и природы спектральная плотность шума в области низких частот (обычно от $10^{-4} < f <$

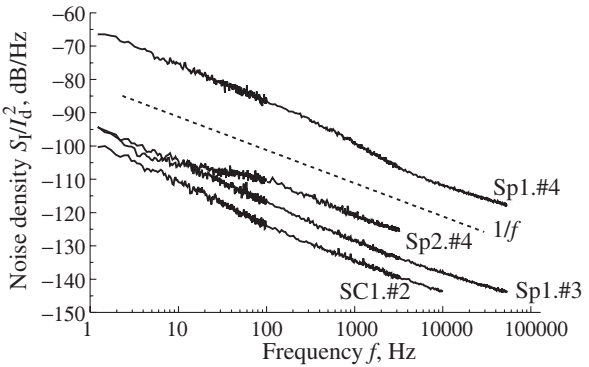

Рис. 1. Пример частотной зависимости спектральной плотности шума типа $1/f$. (Шум в GaN/AlGaN HFETs, выращенных на сапфировых и карбид-кремниевых подложках.) Пунктиром показана зависимость $1/f$.

10^4-10^6 Гц) имеет вид $1/f$: $S_v \propto 1/f$ (Рис. 1).

Далеко не полный список таких объектов включает, например,

- полупроводниковые сопротивления всех типов: n- и p-типов, вырожденные и не вырожденные, собственные и примесные, кристаллические, аморфные, поликристаллические, и т.д.;
- «сопротивления» на основе любых металлов и сплавов;
- частотные, фазовые и амплитудные шумы всех полупроводниковых и практически всех других электронных генераторов, включая атомные стандарты частоты, диоды Ганна, ЛПД, все типы полевых и биполярных транзисторов, лазеры, светодиоды, и т.д.;
- намагниченность всех типов ферро- и антиферромагнетиков;
- потенциалы биологических клеток;
- концентрация инсулина в крови при нестабильном диабете (Рис. 2);
- количество автомашин на автостраде в единицу времени (трафик);
- малоамплитудные осцилляции земной коры;
- прозрачность атмосферы;
- уровень паводкового подъема воды в реке Нил (по данным за $\sim$ 2800 лет);
- музыка (в особенности, классическая), и т.д., и т.д., и т.д., и т.д., и т.д.

Явление такой общности привлекает к себе повышенное внимание со стороны патологов, любителей решать «мировые проблемы» и просто сумасшедших. Поэтому «концентрация» патологических теорий, подходов, гипотез в этой области, хотя и уменьшается со временем, все же достаточна велика и посейчас.

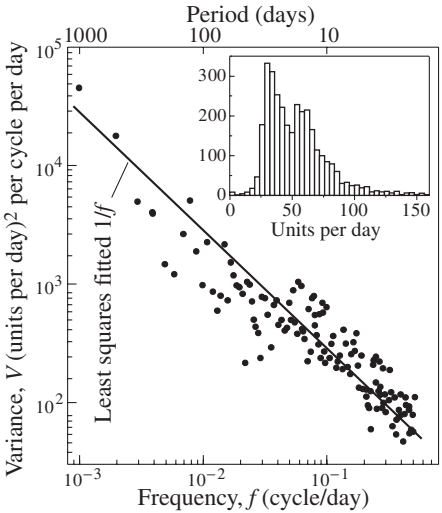

Рис. 2. На вставке показана гистограмма распределения количества инсулина, вводимого ежедневно пациенту, страдающему нестабильным диабетом. (Время наблюдения — 8 лет, всего 3072 доз). На графике показано разложение этой случайной функции в ряд Фурье. Сплошная линия — зависимость $1/f$.

Правда состоит в том, что мы не знаем природы шума $1/f$ в подавляющем большинстве объектов, где он наблюдается. Однако, в тех немногих случаях, когда природа этого шума установлена, например, в ферромагнетиках, многих металлических и полупроводниковых объектах и приборах, этот тип шума возникает вследствие суперпозиции (суммирования) шума от отдельных «флуктуаторов» природа которых, как правило, ясна.

Интегрирование спектральной плотности шума в полосе частот, где превалирует $1/f$ шум, дает мощность, сосредоточенную в этом типе шума. Оценки показывают, что эта мощность лежит в пределах от 10^{-14} (для наиболее стабильных объектов, например, атомных стандартов частоты) до 10^{-5} (для очень «шумных» объектов) от мощности, потребляемой от источника. Несмотря на кажущуюся ничтожность эффекта, шум $1/f$ изучается вот уже почти 80 лет, и число исследователей, вовлеченных в соответствующие работы, монотонно возрастает.

С точки зрения тематики настоящей школы шум $1/f$ наиболее интересен тем, что он очень часто характеризует уровень разупорядоченности полупроводника или металла. При этом шумовые измерения дают возможность обнаруживать дефектность материала с такой чувствительностью, которая оказы-

вается недоступной ни для электрических, ни для оптических методов. В Si, например, уровень шума $1/f$ может изменяться на 5–6 порядков при практически неизменных значениях подвижности и концентрации.

Физическая природа $1/f$ шума имеет много общего с такими явлениями как электромиграция, внутреннее трение, деградация.

Уровень шума $1/f$ определяет предельную обнаружительную способность практически всех типов оптоэлектронных приборов и предельную чувствительность широкополосных налоговых схем. Высокая чувствительность иногда дает возможность по уровню шума $1/f$ на любой стадии изготовления приборов судить о их будущей надежности и долговечности.

Однако, с практической точки зрения, шум $1/f$ важен, прежде всего, потому, что именно он определяет в подавляющем большинстве случаев уровень фазовых и частотных шумов всех СВЧ и оптических генераторов. Низкочастотные флуктуации активного элемента генератора (полевого или биполярного транзистора, ЛПД, диода Шоттки, диода Ганна, и т.д.) преобразуются в шум вблизи несущей частоты генератора (convert up). Чем выше уровень шума $1/f$, тем более широкую полосу частот приходится отводить на один связной канал.

Как упоминалось выше, в тех случаях, когда природа шума $1/f$ установлена, этот тип шума возникает вследствие суперпозиции (суммирования) шума от отдельных «флуктуаторов».

В случае, если случайный процесс характеризуется одной постоянной времени, τ, (элементарный флуктуатор), спектральная плотность шума S имеет вид так называемого «Лоренциана»: $S \propto \frac{\tau}{1+(\omega\tau)^2} = \frac{\tau}{1+(2\pi f\tau)^2}$. На частотах, существенно меньших, чем $f_0 = 1/\tau$, S не зависит от частоты. При $f_0 \gg 1/\tau$, $S \sim 1/\mathrm{f}^2$.

Наиболее простой пример такого рода шума в полупроводниках — генерационно-рекомбинационный (ГР) шум от локального уровня в запрещенной зоне полупроводника (Рис. 3а). *Средняя* концентрация свободных носителей (электронов), «поставляемая» в зону проводимости уровнем, определяется концентрацией уровня, положением уровня Ферми и температурой. Однако, в действительности, эта концентрация флуктуирует, и как следствие, концентрация носителей в зоне может быть и меньше, чем средняя (проводимость образца понижена), и больше, чем средняя (проводимость повышена). Постоянная времени обмена носителями между уровнем и зоной, τ, определяется концентрацией носителей в зоне проводимости, сечением захвата уровня и температурой. Исследуя температурную зависимость шума (Рис. 3б), можно определить энергию активации уровня, сечение захвата и концентрацию центров (шумовая спектроскопия).

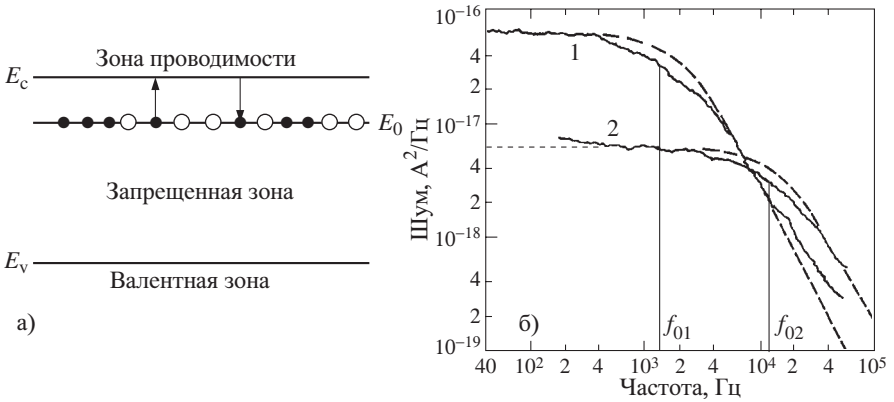

Рис. 3. а) Концентрация свободных носителей (электронов), поставляемая в зону проводимости уровнем в запрещенной зоне, флуктуирует с постоянной времени τ. Как следствие, флуктуирует сопротивление образца.
б) Спектры токовых шумов образца n-GaAs при температуре $T = 241$ К (кривая 1) и 293 К (кривая 2). Штриховые линии соответствуют классическим Лоренцианам: Постоянная времени $\tau = 1/2\pi f_0$ падает с ростом температуры.

Суперпозиция тесно расположенных Лоренцианов (распределенных с надлежащим статистическим весом) может обусловить шум типа $1/f$ (Рис. 4). Действительно, интегрирование в широкой полосе значений τ с функцией распределения $p(\tau)$:

$$S(f) = \int_0^\infty \frac{\tau}{1 + (\omega\tau)^2} p(\tau) d\tau$$

при $p(\tau) \sim 1/\tau$ дает $1/f$ шум во всем диапазоне частот.

Разумеется, для любой реальной системы нет нужды в интегрировании от нуля до бесконечности. Достаточно интегрировать от частот много ниже, чем нижний предел наблюдаемого шума $1/f$ (обычно этот предел составляет $10^{-1}-10$ Гц, в редких случаях $\sim 10^{-3}$ Гц, в уникальных — 10^{-3} Гц), до частот, превышающих верхнюю границу $1/f$ шума (Рис. 4). Обычно эта граница составляет 10^3-10^6 Гц. Однако, найти в реальном объекте источник флуктуаций, обеспечивающий достаточно «плотное» распределение флуктуаторов со значениями τ, меняющимися в пределах 5–10 порядков, как правило, задача нетривиальная. Собственно, в этом и состоит, как правило, реальная, а не параноидальная загадка $1/f$ шума.

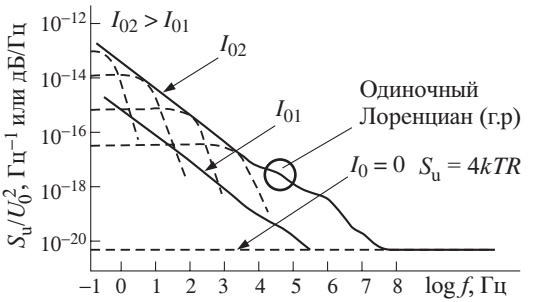

Рис. 4. Суперпозиция тесно расположенных Лоренцианов, распределенных с надлежащим статистическим весом, может обусловить шум типа $1/f$.

Некоторая «подсказка» содержится в виде функции распределения $p(\tau)$. Пусть, например, речь идет о флуктуациях проводимости в полупроводнике или металле. Понятно, что источником шума могут служить флуктуации подвижности и/или флуктуации числа носителей. Предположим, что для того, чтобы носитель на время «выбыл» из проводимости: захватился на центр в объеме, на поверхности, в прилегающем слое окисла, и т.д., он должен преодолеть энергетический барьер с энергией $\varepsilon \gg kT$. Носитель атакует этот барьер с частотой $f_0 = 1/\tau_0$. Характерная постоянная времени преодоления такого барьера $\tau = \tau_0 \exp(\varepsilon/kT)$. Характерная вероятность $p(\tau) \sim \exp(-\varepsilon/kT)$. Как видно, в этом случае $p(\tau) \sim 1/\tau$. Если в материале имеется «набор» барьеров с близко расположенными энергиями ε, возникнет шум типа $1/f$ (модель P. Dutta and P. M. Horn, Rev. Modern Phys. **53**, 497–516, (1981)). Т.о., подсказка состоит в том , чтобы искать экспоненциально широкое распределение возможных постоянных времени τ. Для флуктуаций проводимости со спектром $1/f$ в полупроводниках и металлах известны три физических механизма $1/f$ шума.

Во многих МОП приборах, включая и самый важный прибор современной электроники — MOSFET, проводимость флуктуирует за счет туннелирования и последующего захвата носителей на ловушки, расположенные в окисле. В этом случае экспоненциально широкое распределение постоянных времени τ возникает за счет экспоненциального уменьшения вероятности туннелирования с увеличением расстояния от границы раздела полупроводник-окисел до ловушки (модель A. L. Mc Whorter, in: *Semiconductor Surface Physics* (ed. by R. H. Kingston, Univ. Pennsylvania Press, Philadelphia) p. 207 (1957)).

В металлах и сильно легированных полупроводниках довольно часто шум $1/f$ возникает за счет флуктуаций подвижности, обусловленных изменением за счет температурных флуктуаций пространственного и/или зарядового со-

стояния дефектов. Экспоненциально широкое распределение постоянных времени τ обусловливается наличием спектра дефектов с различными энергиями активации (модель Ш. М. Коган и К.Э. Нагаев, ФТТ, **24**, 3381–3388 (1982)).

В ряде полупроводников (GaAs, Si при пониженных температурах, возможно, GaN) шум $1/f$ обусловлен флуктуациями заселенности уровней, образующих хвост плотности состояний вблизи границ зоны проводимости и валентной зоны. Экспоненциально широкое распределение постоянных времени τ обусловлено многофононным механизмом захвата носителей на уровни в хвостах плотности состояний (Н. В. Дьяконова и М. Е. Левинштейн, ФТП, **23**, 283–291, (1989)).

Даже в таких относительно простых объектах как электронные приборы найти источник шума $1/f$, определить его природу и проследить связь этого явления с другими эффектами, как правило, бывает очень непросто.

В природных и, в особенности, биологических объектах, природа шума $1/f$, как правило, совершенно непостижима. Где «спрятаны» наборы постоянных времени τ, позволяющие реке Нил «помнить», каков был уровень паводка 2800 лет назад? Что человеческий организм может помнить о том, какая доза инсулина была введена 8 лет назад (рис. 2)? Почему спектральное разложение «Бранденбургского Концерта» Баха дает спектр $1/f$?

Между тем, сейчас каждая третья статья о шуме $1/f$ посвящена исследованиям этого феномена в биологии и медицине. Даже не понимая природы явления, из эмпирического анализа шума $1/f$ оказывается возможным установить интересные и полезные закономерности.

Отпечатано с готового оригинал-макета в типографии ПИЯФ РАН
188350, Гатчина Ленинградской обл., Орлова роща
Зак. 65, тир. 170, уч.-изд. л. 5,25, 20.02.2004 г.